

# Cosmic web dependence of galaxy clustering and quenching in SDSS

Shadab Alam<sup>1</sup>\*, Ying Zu<sup>2</sup>†, John A. Peacock<sup>1</sup>‡, and Rachel Mandelbaum<sup>3</sup>§

<sup>1</sup> *Institute for Astronomy, University of Edinburgh, Royal Observatory, Blackford Hill, Edinburgh, EH9 3HJ, UK*

<sup>2</sup> *Department of Astronomy, Shanghai Jiao Tong University, 800 Dongchuan Road, Shanghai, 200240, China*

<sup>3</sup> *Department of Physics and the McWilliams Center for Cosmology, Carnegie Mellon University, 5000 Forbes Ave., Pittsburgh, PA 15213, USA*

15 March 2022

## ABSTRACT

Galaxies exhibit different clustering and quenching properties in clusters, filaments, and the field, but it is still uncertain whether such differences are imprints of the tidal environment on galaxy formation, or if they reflect the variation of the underlying halo mass function across the cosmic web. We measure the dependence of galaxy clustering and quenching on the cosmic web in the Sloan Digital Sky Survey, characterized by the combination of spherical overdensity  $\delta_8$  and tidal anisotropy  $\alpha_5$  centred on each galaxy. We find that galaxy clustering is a strong function of either  $\delta_8$  or  $\alpha_5$ , and the large-scale galaxy bias shows complex and rich behaviour on the  $\delta_8$  vs.  $\alpha_5$  plane. Using the mean galaxy colour as a proxy for the average quenched level of galaxies, we find that galaxy quenching is primarily a function of  $\delta_8$ , with some subtle yet non-trivial dependence on  $\alpha_5$  at fixed  $\delta_8$ . The quenched galaxies generally show stronger small-scale clustering than the star-forming ones at fixed  $\delta_8$  or  $\alpha_5$ , while the characteristic scale at which the amplitude of clustering becomes comparable for both galaxy populations varies with  $\delta_8$  and  $\alpha_5$ . We compare these observed cosmic web dependences of galaxy clustering and quenching with a mock galaxy catalogue constructed from the *i*HOD model, which places quenched and star-forming galaxies inside dark matter haloes based on the stellar-to-halo mass relation and the halo quenching model — the  $\delta_8$  and  $\alpha_5$  dependences of *i*HOD galaxies are thus solely derived from the cosmic web modulation of the halo mass function. The main observed trends are accounted for extremely well by the *i*HOD model. Thus any additional direct effect of the large-scale ( $>5 h^{-1}\text{Mpc}$ ) tidal field on galaxy formation must be extremely weak in comparison with the dominant indirect effects that arise from the environmental modulation of the halo mass function.

**Key words:** gravitation; galaxies: statistics, Quenching; large-scale structure of Universe;

## 1 INTRODUCTION

The 3D distribution of galaxies in our Universe exhibits a visually striking web-like pattern, consisting of dense knots of galaxies as groups and clusters, connected by filaments and sheets, with vast regions of cosmic voids in between (Bond et al. 1996). This so-called ‘cosmic web’ formed naturally out of the Gaussian initial density field within  $\Lambda$ CDM (White et al. 1987); this is a somewhat surprising outcome considering that large-scale structure formed hierarchically through the merging and accretion of dark matter haloes (Peebles 1980), rather than the fragmentation of giant ‘pancakes’ (Zel’dovich 1970; Sunyaev & Zel’dovich 1972) — an intuitively more straightforward mechanism for generating sheet-like structures. One of the key questions to ask is whether the properties of haloes and galaxies depend on the local cosmic web environment. Some such dependence is inevitable through the ‘peak-

background split’, which states that the mass function of haloes is modified by the large-scale density contrast (Kaiser 1984; Sheth & Tormen 1999); thus it is inevitable that e.g. voids will be deficient in massive galaxies. But beyond this leading-order effect, is there any evidence that the cosmic web causes the galaxy population within it to change with location? In other words, at a fixed density contrast, is there any impact on the galaxy properties by the different tidal forces that are found in different geometrical locations within the web? In principle, a hypothetical effect of this sort might modulate the halo mass function beyond the predictions of the peak-background split. But even if it does not do so, it is possible that the mean galaxy content of a halo of a given mass might depend on cosmic web location in addition to the halo mass. For example a massive halo close to a filament could slow down the growth of smaller halos in its vicinity (Hahn et al. 2009; Borzyszkowski et al. 2017; Castorina et al. 2016) and a large scale tidal field alone can introduce a gradient in the accretion rate of halos (Musso et al. 2018). Such cosmic-web effects are presumed to be absent according to the widely-used halo model framework (Jing et al. 1998; Ma & Fry 2000; Seljak 2000; Peacock & Smith 2000;

\* salam@roe.ac.uk

† yingzu@sjtu.edu.cn

‡ jap@roe.ac.uk

§ rmandelb@andrew.cmu.edu

Benson et al. 2000; Scoccimarro et al. 2001; Berlind & Weinberg 2002; Cooray & Sheth 2002; Yang et al. 2003; Kravtsov et al. 2004; Zheng et al. 2005; Mandelbaum et al. 2006; Leauthaud et al. 2011), and the main aim of the present paper is to test this assumption. We therefore measure the cosmic web dependence of the clustering and quenching properties of galaxies in the Sloan Digital Sky Survey (SDSS; York et al. 2000), and compare our results to the predictions from a cosmic-web agnostic mock galaxy catalogue built from the improved Halo Occupation Distribution model ( $\text{iHOD}$ ; Zu & Mandelbaum 2015, 2016, 2017).

The clustering of dark matter haloes has an extremely complicated dependence on the cosmic web environment. By measuring the halo-dark matter cross-correlation and halo-halo auto-correlation functions across four types of cosmic web environments (clusters, filaments, sheets, and voids), Yang et al. (2017b) and Xia et al. (2017) found that on scales larger than  $8 h^{-1} \text{Mpc}$  the clustering bias of Milky Way-size haloes is significantly enhanced in voids, but strongly suppressed in cluster environments (see their Figure 7). Using the SDSS main galaxy sample, Abbas & Sheth (2007) also discovered a non-monotonic trend of galaxy clustering with galaxy spherical overdensity, confirming the theoretical expectation from the linear peaks bias model (Kaiser 1984; Sheth 1998). However, they found that the non-trivial scale and overdensity dependences of galaxy clustering can be well reproduced by a simple three-parameter HOD model that depends only on halo mass, suggesting that the observed dependences largely stem from the density dependence of the halo mass function (HMF). We will extend the analysis of Abbas & Sheth (2007) to measure the dependence of galaxy clustering on the tidal anisotropy of the cosmic web environment, and look for evidence of any deviation from the  $\text{iHOD}$  predictions. Such a deviation would be direct evidence that the HOD of galaxies depends not only on halo mass, but also on the properties of the cosmic web — a form of the so-called ‘galaxy assembly bias’ (Croton et al. 2007; Tinker et al. 2008; Zu et al. 2008; Wang et al. 2013; Lin et al. 2016; Zentner et al. 2016; Tojeiro et al. 2017; Guo et al. 2017; Zehavi et al. 2017). Past searches for such effects have not reported any strong impact of the anisotropic tidal field within the cosmic web on the mass function of the dark matter haloes (Alonso et al. 2015) or on the luminosity function of galaxies (Eardley et al. 2015). However, our work differs from these studies by using a different measure of the tidal field, and we also focus on the distinct question of galaxy quenching.

Halo mass is taken to be one of the main drivers of galaxy quenching in theoretical models (Dekel & Birnboim 2006; Cattaneo et al. 2006; Correa et al. 2018). Observationally, Zu & Mandelbaum (2016) found that the halo quenching model provides significantly better fits to the clustering and galaxy–galaxy lensing of SDSS galaxies than the other models that tie quenching to stellar mass or halo age. The fiducial  $\text{iHOD}$  halo quenching model also correctly predicts the average halo mass of the red and blue centrals, showing excellent agreement with the direct weak lensing measurements (Mandelbaum et al. 2016). The  $\text{iHOD}$  modelling of galaxy colours provides strong evidence that the physical mechanism that quenches star formation in galaxies above stellar masses of  $10^{10} h^{-2} M_{\odot}$  is tied principally to the masses of their dark matter haloes, rather than the properties of their stellar components or halo age.

Besides halo mass, the cosmic web may also play a significant role in the quenching of star formation in galaxies. In particular, hydrodynamic simulations predict that the cold gas flow is often directed along filaments (Kereš et al. 2005), allowing galaxies to efficiently accrete gas from large distances and sustain star

formation (Kleiner et al. 2017). Aragon-Calvo et al. (2016) speculated that the stripping of the filamentary web around galaxies is the physical process responsible for quenching star formation, as cold gas stripping, harassment, strangulation and starvation often happened during the so-called ‘cosmic web detachment’ events. Therefore, it is very important to understand the relative impact of the cosmic web on galaxy quenching compared to that of halo mass (Metuki et al. 2015).

Recent studies of cosmic-web quenching mainly focused on the quenched fraction of galaxies as a function of distance to the filaments. Using the GAMA survey, Kraljic et al. (2017) found that the red (i.e., quenched) fraction increases when approaching knots and filaments, and the star-forming population reddens at fixed mass when approaching filaments (see also Guo et al. 2015b; Alpaslan et al. 2016; Chen et al. 2017; Kuutma et al. 2017; Malavasi et al. 2017; Poudel et al. 2017; Crone Odekon et al. 2017). In order to try to disentangle the effect of overdensity from that of the anisotropic tides, Kraljic et al. shuffled the colours of galaxies at the same overdensity and stellar mass to preserve the colour-density-mass relation while erasing any cosmic web effects. They found the cosmic web dependence of galaxy colours substantially reduced in the reshuffled catalogue, suggesting some unexplained tidal impact on galaxy quenching. However, it is very challenging to disentangle further the effect of cosmic web from that of halo mass using this shuffling technique, as the mass of individual haloes is inaccessible from observations.

To distinguish between the cosmic web and halo mass effects on galaxy formation, we build a mock galaxy catalogue by implementing the  $\text{iHOD}$  prescription of Zu & Mandelbaum (2015) and the fiducial halo quenching model of Zu & Mandelbaum (2016, 2017), without any explicit cosmic-web effect in galaxy clustering or quenching. Any effect of the cosmic web on halo formation and the halo mass function is implicitly taken into account by using haloes from N-body simulations. This  $\text{iHOD}$  halo quenching model correctly reproduces the stellar mass and colour dependence of galaxy abundance, spatial clustering, and galaxy–galaxy lensing, as well as the conformity of galaxy colours (Zu & Mandelbaum 2017), therefore serving as an ideal cosmic-web agnostic benchmark model to compare with observations — any observed cosmic web dependences of galaxy clustering and quenching that are unexplained by this  $\text{iHOD}$  halo quenching model would provide important clues as to what aspect of galaxy formation was shaped by the cosmic web. Similar  $\text{iHOD}$  halo quenching mock catalogues were constructed by Zu et al. (2017) and Calderon et al. (2017) to study cluster assembly bias and galaxy conformity, respectively.

The cosmic web is usually decomposed into four structural elements — knots, filaments, sheets, and voids, based on the Hessian of the pseudo-gravitational potential computed from the galaxy distribution (Hahn et al. 2007). Unfortunately, the classification of any fixed galaxy position is not unique, but depends on the choice of thresholds in the eigenvalues of the Hessian (Libeskind et al. 2018). To circumvent this problem of arbitrariness during the classification, we adopt the combination of two orthogonal parameters: the spherical overdensity, and the ‘tidal anisotropy’ recently proposed by Paranjape et al. (2017) to characterize the underlying cosmic web environment of each galaxy. Another advantage of this method of characterizing the cosmic web is that the two parameters are continuous variables, therefore allowing us to bin galaxies arbitrarily on the 2D parameter plane.

The paper is organized as follows. We first introduce the SDSS data and  $\text{iHOD}$  mock catalogues used in our analysis in section 2. In section 3 we describe the technique used to compute galaxy over-

density and tidal anisotropy in the two catalogues. We then discuss our results by comparing the observations to  $\text{iHOD}$  predictions in section 4. We conclude by summarizing our results and discussing their implications in section 5. We assume a flat  $\Lambda\text{CDM}$  cosmology with  $\Omega_m=0.30$  unless specified otherwise. We also use  $\lg$  to denote  $\log_{10}$  everywhere in the text.

## 2 DATA AND MOCK GALAXY CATALOGUES

In this section we briefly describe the data and mock galaxies used in this paper, including the selection of the stellar mass-thresholded volume-limited galaxy catalogue from SDSS in Section 2.1, and the construction of the  $\text{iHOD}$  mock galaxy catalogue based on the halo quenching model in Section 2.2. For technical details in the making of the two catalogues, we refer readers to [Zu & Mandelbaum \(2015, 2016\)](#) for the SDSS data, and [Zu & Mandelbaum \(2017\)](#) for the  $\text{iHOD}$  mock, respectively.

### 2.1 SDSS NYU-VAGC galaxy catalogue and sample selection

We make use of the final data release of the SDSS I/II (DR7; [Abazajian et al. 2009](#)), which contains the completed data set of the SDSS-I and the SDSS-II. In particular, we obtain the Main Galaxy Sample (MGS) data from the `dr72` large-scale structure sample `bright0` of the ‘New York University Value Added Catalogue’ (NYU-VAGC), constructed as described in [Blanton et al. \(2005\)](#). We apply the ‘nearest-neighbour’ scheme to correct for the 7% of galaxies that are without redshifts due to fibre collisions, and use data exclusively within the contiguous area in the North Galactic Cap and regions with angular completeness greater than 0.8.

We employ the stellar mass estimates from the latest MPA/JHU value-added galaxy catalogue<sup>1</sup>. The stellar masses were estimated based on fits to the SDSS photometry following the methods of [Kauffmann et al. \(2003\)](#) and [Salim et al. \(2007\)](#), and assuming the Chabrier ([Chabrier 2003](#)) Initial Mass Function (IMF) and the [Bruzual & Charlot \(2003\)](#) Stellar Population Synthesis (SPS) model.

For the purpose of our analysis, we select all the SDSS galaxies within the redshift range  $z=[0.01, 0.074]$  and with stellar mass above  $M_*^{\min}=10^{10} h^{-2} M_\odot$ , yielding a sample of 65222 galaxies in total. Based on the stellar mass completeness limit estimated in [Zu & Mandelbaum \(2015\)](#), we believe this galaxy sample is roughly volume-complete down to  $M_*^{\min}$ , therefore can be used to directly compare with any mock galaxy samples thresholded by  $M_*^{\min}$ .

### 2.2 iHOD Mock galaxy catalogue with halo quenching

We employ the ‘fiducial  $\text{iHOD}$  halo quenching mock’ of [Zu & Mandelbaum \(2017\)](#) as our mock galaxy catalogue to compare with the data. For the purpose of this paper, we use a cosmological dark matter-only Bolshoi ([Klypin et al. 2011](#)) simulation because of its high dark matter mass resolution ( $1.35 \times 10^8 h^{-1} M_\odot$ ) and relatively large volume ( $250^3 h^{-3} \text{Mpc}^3$ ). We make use of the halo catalogues identified by the ROCKSTAR ([Behroozi et al. 2013](#)) spherical overdensity halo finder at  $z=0.1$ . Finally, we populate the halo catalogue with mock galaxies and assign them stellar mass and  $g-r$  colours using the same parameters as in [Zu & Mandelbaum \(2017\)](#).

We have implemented the best-fitting velocity bias model of [Guo et al. \(2015a\)](#), which assumes that the relative velocities of central and satellite galaxies follow Gaussian distributions within each halo.

In particular, the central galaxies and their host haloes follow a mean stellar-to-halo mass relation (SHMR), with a log-normal scatter that is also dependent on halo mass. Each halo also hosts a number of satellite galaxies according to a conditional stellar mass function that only depends on the mass of that halo, with their relative positions following an isotropic NFW distribution. Therefore, the stellar mass assignment in the  $\text{iHOD}$  mock is tied only to the mass of host haloes, independent of the overdensity or tidal anisotropy of the cosmic web environment.

To assign  $g-r$  colours to the mock galaxies at fixed  $M_*$  and  $M_h$ , we adopt the fiducial halo quenching prescription described in [Zu & Mandelbaum \(2017\)](#), so that the ranking order of galaxy colours at fixed  $M_*$  depends only on halo mass. The colour ranks are then converted to  $g-r$  values according to the observed colour distribution at that  $M_*$ . As a result, the quenching properties of the mock galaxies, as measured by the simulated  $g-r$  colours, also depend only on the halo mass.

## 3 GALAXY ENVIRONMENTAL CLASSIFICATION

In order to make a quantitative characterization of the cosmic web, we need to create a robust estimate of the tidal tensor field using galaxies as tracers. We use the tidal tensor formalism developed in [Hahn et al. \(2007\)](#) (see also [Forero-Romero et al. 2009](#); [Eardley et al. 2015](#)), and apply the method to both the SDSS data and  $\text{iHOD}$  mock catalogues. In the rest of this Section we will describe the technical details of the estimation method, but readers who are familiar with the method can skip to § 3.4 for the definition of  $\delta_8$  and  $\alpha_5$  based on the estimated tidal tensor field.

### 3.1 Data regularization

The first step of deriving the tidal tensor field is to solve the Poisson equation, which can be done efficiently in  $k$ -space using fast Fourier transforms. Naively, such procedure would require placing the entire survey volume inside an encapsulating box. However, surveys like the SDSS usually consist of a light-cone that extends to  $200 h^{-1} \text{Mpc}$  along the line-of-sight, with a large fraction of the volume being empty. Therefore, to avoid having such a large box we regularize the survey volume and discard galaxies outside our regularized volume for efficiency purposes. We first calculate the 3D Cartesian coordinates for all galaxies assuming our fiducial cosmology, and examine the galaxy number distribution along each of the three axes by using a histogram with 500 bins. For each axis, we then find the threshold coordinate value by choosing the bins with number of galaxy 10% of the bin with highest number of galaxy. The cut-off threshold of 10% is chosen empirically, so that we can keep 98.5% of the total galaxies while minimizing the volume of the encapsulating box. This leaves us with a box of size  $195 \times 340 \times 198 h^{-1} \text{Mpc}$  with 65% of the volume containing the galaxies, and the rest is empty.

### 3.2 Density estimation

After the regularization, we compute the local density field using a hybrid scheme based on the Voronoi tessellation of the observed

<sup>1</sup> <http://home.strw.leidenuniv.nl/~jarle/SDSS/>

galaxy catalogue, for which an accompanying random galaxy catalogue has to be generated to account for the survey mask and window function. Voronoi tessellation has been widely used in modern cosmology for computing the galaxy density fields, providing a grid-free way of estimating density (van de Weygaert 2012) as opposed to count-in-cell methods. During the tessellation the survey volume is partitioned such that the volume element closest to a given galaxy is assigned to that galaxy, yielding a non-overlapping volume for each galaxy after combining all the volume elements belong to that galaxy. We can then estimate the density at the location of each galaxy by computing the inverse of the total volume associated with that galaxy.

However, in actual surveys the footprint usually has sharp boundaries, as well as holes inside the boundaries that are masked out due to bright stars and/or bad seeing, so it could be difficult to account for the missing area during tessellation. One approach to overcome this problem was proposed by Sutter et al. (2015), who associated the volume outside the immediate survey boundaries with mock galaxies rather than any of the observed galaxies. This method is hard to implement, requiring the generation of mock galaxies whose spatial distribution is statistically consistent with that of the observed ones. Instead, we exploit the random galaxy catalogue that encodes the same angular and redshift selection functions of the observed galaxies, and estimate density by directly counting the number of nearest random galaxies around each observed galaxy.

For any galaxy near the survey boundaries or masks, we estimate the density at the location of that galaxy using the inverse of the total number of closest randoms up to a constant multiplicative normalization factor. This scheme inherits all the advantages of the traditional tessellation method, but is subject to sampling noise of random points — the noise in the density estimates depends on the total number of randoms used. In general, such a method can be implemented very efficiently by using tree-based algorithms, which enable the use of very large number of randoms, rendering the statistical noise negligible.

### 3.3 Tidal tensor and eigenvalues

After we estimate the local densities at the galaxy positions, we interpolate the density field on a regular grid, which is then smoothed with a Gaussian kernel of width  $5 h^{-1} \text{Mpc}$ . Ideally, the tidal anisotropy should be evaluated at a few times the halo size (Paranjape et al. 2017), providing the redshift space smoothed density  $\delta_g^s$  on a grid. We can then relate  $\delta_g^s$  to the gravitational potential  $\Phi$  through the Poisson equation under the linear bias assumption

$$\nabla^2 \Phi = 4\pi G \bar{\rho} \delta_g^s / b_g, \quad (1)$$

where  $G$  is the gravitational constant,  $b_g$  is galaxy bias and  $\bar{\rho}$  is the mean matter density. We note that above equation only applies in real space, but we ignore this and do not try to correct for redshift space. This is a reasonable assumption on large linear scales, which is why  $5 h^{-1} \text{Mpc}$  filtering is performed. The above equation can be rewritten in terms of the dimensionless gravitational potential ( $\tilde{\Phi}$ ):

$$\nabla^2 \tilde{\Phi} = \delta_g^s. \quad (2)$$

What we are really interested in is the dynamical evolution of two test particles (in this case, two galaxies) that are placed close to a given location. In essence, the dynamics will be determined by the relative gravitational acceleration between the two particles due to

tidal force. The net force on a particle is given by the negative gradient of the potential, while the relative acceleration is given by the gradient of the force, which is the second derivative of the gravitational potential. In 3D space we can write the nine components of this tidal force, i.e., the tidal tensor matrix  $\tilde{T}^s$ , as

$$\tilde{T}^s = \begin{bmatrix} \partial^2 \tilde{\Phi} / \partial x^2 & \partial^2 \tilde{\Phi} / \partial x \partial y & \partial^2 \tilde{\Phi} / \partial x \partial z \\ \partial^2 \tilde{\Phi} / \partial y \partial x & \partial^2 \tilde{\Phi} / \partial y^2 & \partial^2 \tilde{\Phi} / \partial y \partial z \\ \partial^2 \tilde{\Phi} / \partial z \partial x & \partial^2 \tilde{\Phi} / \partial z \partial y & \partial^2 \tilde{\Phi} / \partial z^2 \end{bmatrix}. \quad (3)$$

The above matrix describes the relative tidal force felt by an infinitesimally close pair of particles. To classify galaxy locations into different geometric environments, we can simply count the number of positive vs. negative eigenvalues of the local tidal tensor. The positive eigenvalues correspond to the directions along which the particles will come closer, hence the collapsing direction, whereas the negative eigenvalues represent the expanding directions. The tidal tensor matrix requires second order partial numerical derivatives which are difficult to compute with noisy data, but we can use the standard Fourier transform-based technique to solve for the components of the matrix in  $k$ -space. We first apply Fourier transform to Equation (2) on both sides, yielding a simple solution for the tidal tensor components in Fourier space:

$$\tilde{T}_{ij}^k = \frac{\partial^2 \tilde{\Phi}^k}{\partial_i \partial_j} = \frac{k_i k_j \delta_g^k}{k^2}, \quad (4)$$

where  $\tilde{\Phi}^k$  and  $\delta_g^k$  are the Fourier transforms of the gravitation potential and density field, respectively.

In summary, to compute the matrix in Equation (3), we first estimate the density at each galaxy location following the procedures described in 3.2. These densities are then interpolated onto a regular grid of  $5 h^{-1} \text{Mpc}$  cell size, which can be smoothed with a Gaussian kernel to remove any discontinuities in the regions with missing data. We use the fast Fourier transform (FFT) package in Python to transform the density field and estimate the tidal tensor components  $\tilde{T}_{ij}^k$ . Finally, each of the tidal tensor components is estimated on a grid, and then inverse Fourier transformed to obtain the tidal tensor in real space, as shown in Equation (3).

### 3.4 Overdensity and tidal shear

As alluded to in the Introduction, we choose the combination of two continuous variables as a measure of the cosmic web environment at each galaxy location. In particular, we define the first parameter  $\delta_8$  as the overdensity of galaxies enclosed within a sphere of radius  $8 h^{-1} \text{Mpc}$ ,

$$\delta_8 = \frac{n_g^8 - \langle n_g \rangle}{\langle n_g \rangle}, \quad (5)$$

where  $n_g^8$  is the 3D number density of galaxies within the  $8 h^{-1} \text{Mpc}$ -radius sphere and  $\langle n_g \rangle$  is the average galaxy number density of the sample. We adopt the  $8 h^{-1} \text{Mpc}$  radius as it is large enough that the impact of small scale velocity dispersion (fingers of god) is negligible. But the effect of large scale ‘Kaiser anisotropy’ will still exist. We choose to avoid any model-dependent correction for this and work with apparent quantities in redshift space that contain uncorrected Kaiser anisotropies. To compute  $\delta_8$ , we first generate 500 random points inside a sphere of radius  $8 h^{-1} \text{Mpc}$  around each galaxy, and derive the densities at those random locations by interpolating the grid values of the density field (as calculated in § 3.2). We then obtain the local density  $n_g^8$  by averaging over all the random points, and compute  $\delta_8$  from Equation (5).



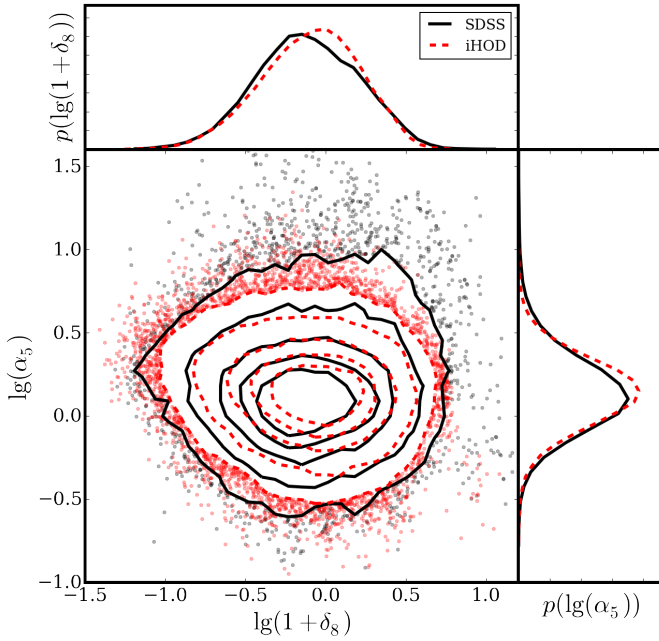


**Figure 1.** Comparison between the 2D distributions of SDSS (black solid) and iHOD (red dashed) galaxies on the  $\delta_8$ - $\alpha_5$  plane. The contour levels are 98%, 90%, 70%, 50% and 30% inwards. The two sub-panels on the right and on the top show the marginalized 1D distributions of  $\lg(\alpha_5)$  and  $\lg(1 + \delta_8)$ , respectively. Note that the distribution of the iHOD galaxies matches that of the SDSS sample quite well, and by construction  $\alpha_5$  is uncorrelated with  $\delta_8$ .

To complement  $\delta_8$ , we need a second parameter to describe the anisotropy level of the cosmic web, and the tidal torque ( $q_R^2$ ) is one such variable proposed in the past (Heavens & Peacock 1988; Catelan & Theuns 1996), defined as

$$q_R^2 = \frac{1}{2}[(\lambda_3 - \lambda_2)^2 + (\lambda_3 - \lambda_1)^2 + (\lambda_2 - \lambda_1)^2], \quad (6)$$

where  $\lambda_{1,2,3}$  are the eigenvalues of the tidal tensor defined in Equation (3), and we adopt the convention that  $\lambda_1 < \lambda_2 < \lambda_3$ . The tidal torque is independent of  $\delta_8$  for a Gaussian random field but not in the case of non-linear structure formation as we see in the real universe (see section 3.2 of Paranjape et al. 2017). To remove the correlation between the tidal anisotropy and overdensity, recently Paranjape et al. (2017) proposed a new ‘tidal anisotropy’ parameter  $\alpha_R$ , which they defined as  $\alpha_R \equiv \sqrt{q_R^2(1 + \delta_R)^{-n}}$ . They adopted  $n=1$  based on empirical tests using simulations and set  $R=4R_{200b}$ , where  $R_{200b}$  is the radius within which enclosed matter density is 200 times the background density. However, in real data we do not have  $R_{200b}$  for each galaxy, so we use a constant smoothing scale  $R=5 h^{-1}\text{Mpc}$  in our analysis. Additionally, the correlation between  $\delta_8$  and  $\alpha_R$  depends on the smoothing scale and the bias of the galaxy sample, so we adjust  $n$  to be 0.55 in the definition of  $\alpha_R$ , thereby eliminating any correlation between  $\delta_8$  and  $\alpha_R$ . The value of  $n = 0.55$  was determined by trying several values and looking for minimum correlation between  $\alpha_5$  and  $\delta_8$ . In the end we have

$$\alpha_5 = \sqrt{q_5^2(1 + \delta_5)^{-0.55}}, \quad (7)$$

where  $\delta_5$  is the galaxy overdensity within a sphere of radius  $5 h^{-1}\text{Mpc}$  centred on each galaxy, computed in the same way as  $\delta_8$ . The value of  $\alpha_5$  determines the spherical symmetry of the tidal and density field. Small  $\alpha_5$  values correspond to isotropic regions

containing voids and clusters. Intermediate values correspond to sheets and filaments and large values of  $\alpha_5$  correspond to the filamentary (anisotropic) regions (see Figure 4 of Paranjape et al. 2017). We measure  $\delta_8$  and  $\alpha_5$  for each galaxy in the mock using the same methods as in the data, so that any systematic uncertainties associated with the measurements (e.g., the effect of the smoothing scales and peculiar velocities) would not affect the results of our comparison between the two catalogues. There can be some subtle residual difference between the data and mock due to differences in cosmological parameters and strength of the Fingers of God (FoG) effect. The clusters with a strong FoG effect can resemble a filamentary structure in redshift space and might lie in high  $\alpha_5$  region rather than the low  $\alpha_5$  region corresponding to the isotropic environment. If this effect is significant then we should see a discrepancy in both high and low  $\alpha_5$  regions.

Figure 1 shows the joint distribution of  $\delta_8$  and  $\alpha_5$  for SDSS (black solid) and iHOD (red dashed) galaxies. In the main panel, the contour levels are 98%, 90%, 70%, 50%, and 30% running inwards. The two subpanels on the right and top show the 1D marginalized distributions of  $\lg(\alpha_5)$  and  $\lg(1 + \delta_8)$ , respectively. As expected,  $\alpha_5$  and  $\delta_8$  show little correlation between each other, thereby providing almost orthogonal information on the local cosmic-web environment. The overall distribution of the iHOD galaxies is in good agreement with that of the SDSS galaxies on the 2D parameter plane, except in the high- $\delta_8$  and high- $\alpha_5$  region where the mock galaxies are slightly under-populated. We selected these outlier galaxies from data with  $\lg(1 + \delta_8) > 0.3$  and  $\lg(\alpha_5) > 1$  where we found a very small number of mock galaxies. We found that these galaxies are clustered together and lie between redshifts of 0.06 and 0.075. We counted the number of galaxy groups and galaxy clusters from NED<sup>2</sup> around these outlier galaxies and found that probability of finding more than 4 clusters within 1 degree is  $0.70 \pm 0.09$ . In contrast, the probability of finding more than 4 clusters within a degree for a typical galaxy within the same redshift is  $0.25 \pm 0.07$  and the probability of finding more than 4 clusters within a degree of random points within the survey footprint is  $0.07 \pm 0.02$ . The uncertainty on the probability includes cosmic variance estimated based on N-body simulation by looking at the variance in the number of haloes above mass  $10^{14} h^{-2} M_\odot$  in equivalent sub-volumes. Therefore we suggest that the excess of data galaxies with high- $\delta_8$  and high- $\alpha_5$  is associated with regions with large number of galaxy clusters and galaxy groups probably forming a massive supercluster, a form of cosmic variance effect that is difficult to capture in the iHOD mock due to its limited volume (but see Wang et al. 2016; Yang et al. 2017a, for an interesting example of constrained simulation to resolve this mismatch.).

<sup>2</sup> The catalogue of galaxy group and galaxy clusters between the redshift of 0.06 and 0.075 were downloaded from <https://ned.ipac.caltech.edu/>

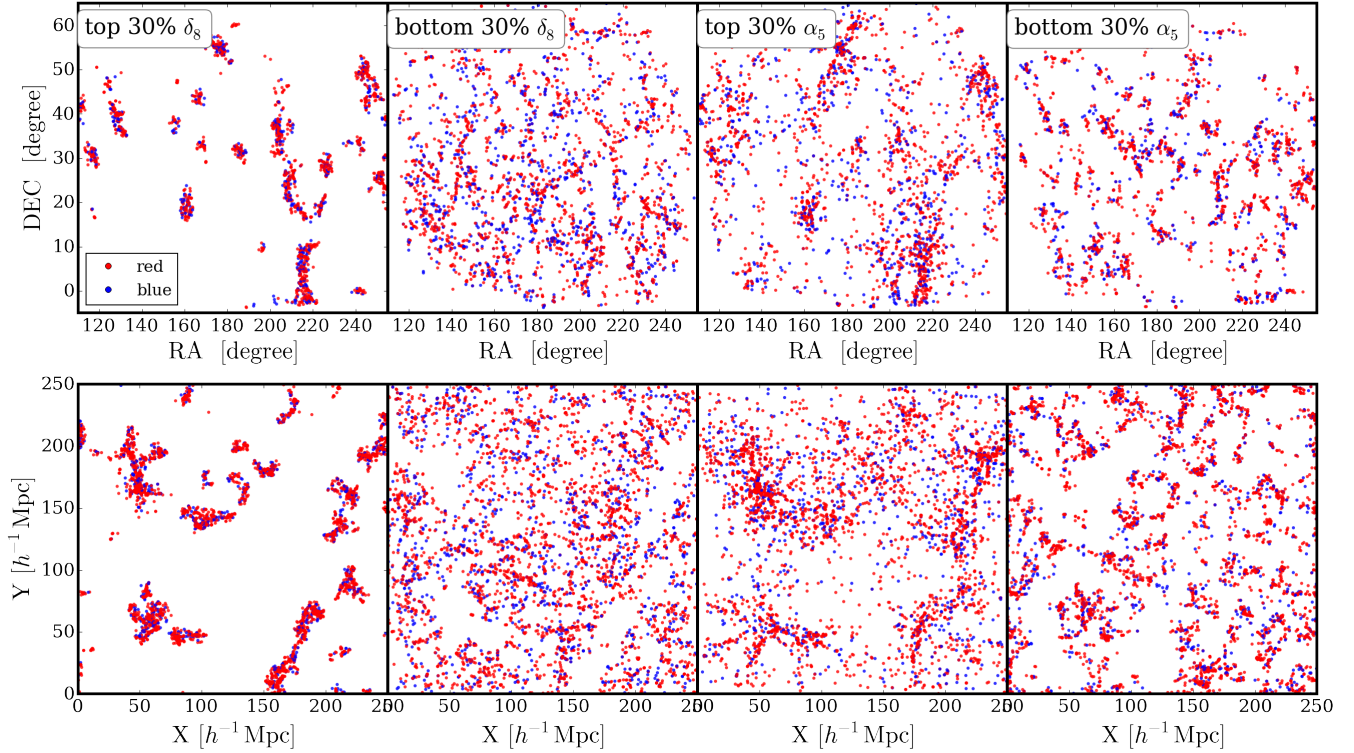


**Figure 2.** The spatial distributions of SDSS (top row) and iHOD (bottom row) galaxies in the top/bottom 30% of  $\delta_8$  (left two columns) and  $\alpha_5$  (right two columns), respectively. The red and blue points indicate the positions of galaxies with red and blue  $g - r$  colours, respectively. The line-of-sight thickness of both samples is  $20 h^{-1} \text{Mpc}$ . The RA/DEC ranges of the SDSS sample are chosen so that the SDSS galaxies subtend approximately  $210 h^{-1} \text{Mpc}$  at the median redshift ( $z = 0.057$ ) of the slice. This figure demonstrates the visual similarity between the galaxy distributions in the SDSS and the iHOD galaxies mock catalogues as a function of environment.

#### 4 RESULTS

Due to the orthogonality between  $\delta_8$  and  $\alpha_5$ , the combination of the two provides a compact yet comprehensive measure of the cosmic web environment for each galaxy. In particular, for any two galaxies at the same  $\delta_8$ , the one with the larger value of  $\alpha_5$  is more likely to live in an anisotropic environment like a filament or a sheet, while the one with the smaller value of  $\alpha_5$  is more likely to be found in a relatively isotropic environment, which is a knot if  $\delta_8$  is high, or a void in the low- $\delta_8$  case. Therefore, if galaxy clustering and quenching have extra dependence on the cosmic web environment beyond halo mass, at fixed  $\delta_8$  and  $\alpha_8$  the SDSS galaxies should have a different spatial distribution and red galaxy fraction than the iHOD mock galaxies.

Figure 2 shows a visual comparison between the spatial distributions of red vs. blue galaxies in four different types of environments within the SDSS (top) and iHOD (bottom) catalogues. In the top row, we show the entire SDSS footprint within the northern galactic cap (i.e., a comoving area approximately  $210 h^{-1} \text{Mpc} \times 210 h^{-1} \text{Mpc}$ ) with a redshift range  $\Delta z = 0.007$  centred at  $0.057$  ( $\approx 20 h^{-1} \text{Mpc}$ ). For the iHOD galaxies we select a slab of dimension  $250 h^{-1} \text{Mpc} \times 250 h^{-1} \text{Mpc} \times 20 h^{-1} \text{Mpc}$ , slightly larger than the SDSS footprint. The different columns show the top and bottom 30% of galaxies in  $\delta_8$  or  $\alpha_5$  (marked on the top left of each panel), and the red and blue points indicate galaxies with red and blue  $g - r$  colours, respectively. As we expected, the volumes occupied by the highest and lowest  $\delta_8$  galaxies correspond to clusters/groups (first column) and voids/fields (second

column), respectively. Meanwhile, the top 30%  $\alpha_5$  galaxies trace the most prominent filamentary structures within the cosmic web, while those with the bottom 30%  $\alpha_5$  have contributions from both the cluster regions and the voids. Overall, the distributions of SDSS and iHOD galaxies exhibit very similar patterns when selected based  $\delta_8$  or  $\alpha_5$ , and we will compare the two in a quantitative fashion in the following sections.

##### 4.1 Dependence of galaxy clustering on $\delta_8$ and $\alpha_5$

We quantify the spatial clustering of galaxies using the projected correlation function  $w_p$ . To derive  $w_p$ , the first step is to compute the 2D correlation function measured in bins of pair separations both parallel ( $r_{\parallel}$ ) and perpendicular ( $r_p$ ) to the line-of-sight direction, using the Landy-Szalay estimator (Landy & Szalay 1993),

$$\xi^{\text{LS}}(r_p, r_{\parallel}) = \frac{DD(r_p, r_{\parallel}) - 2DR(r_p, r_{\parallel}) + RR(r_p, r_{\parallel})}{RR(r_p, r_{\parallel})}, \quad (8)$$

where  $DD$ ,  $DR$ , and  $RR$  represent the number counts of galaxy-galaxy pairs, galaxy-random pairs, and random-random pairs, respectively. We use 20 logarithmic bins in  $r_p$  (between  $0.1$  and  $30 h^{-1} \text{Mpc}$ ) and 40 linear bins in  $r_{\parallel}$  (between  $-40$  and  $40 h^{-1} \text{Mpc}$ ). We then integrate  $\xi^{\text{LS}}(r_p, r_{\parallel})$  along the line-of-sight to obtain  $w_p$ ,

$$w_p = \int_{r_{\parallel}=-40}^{r_{\parallel}=40} dr_{\parallel} \xi^{\text{LS}}(r_p, r_{\parallel}). \quad (9)$$

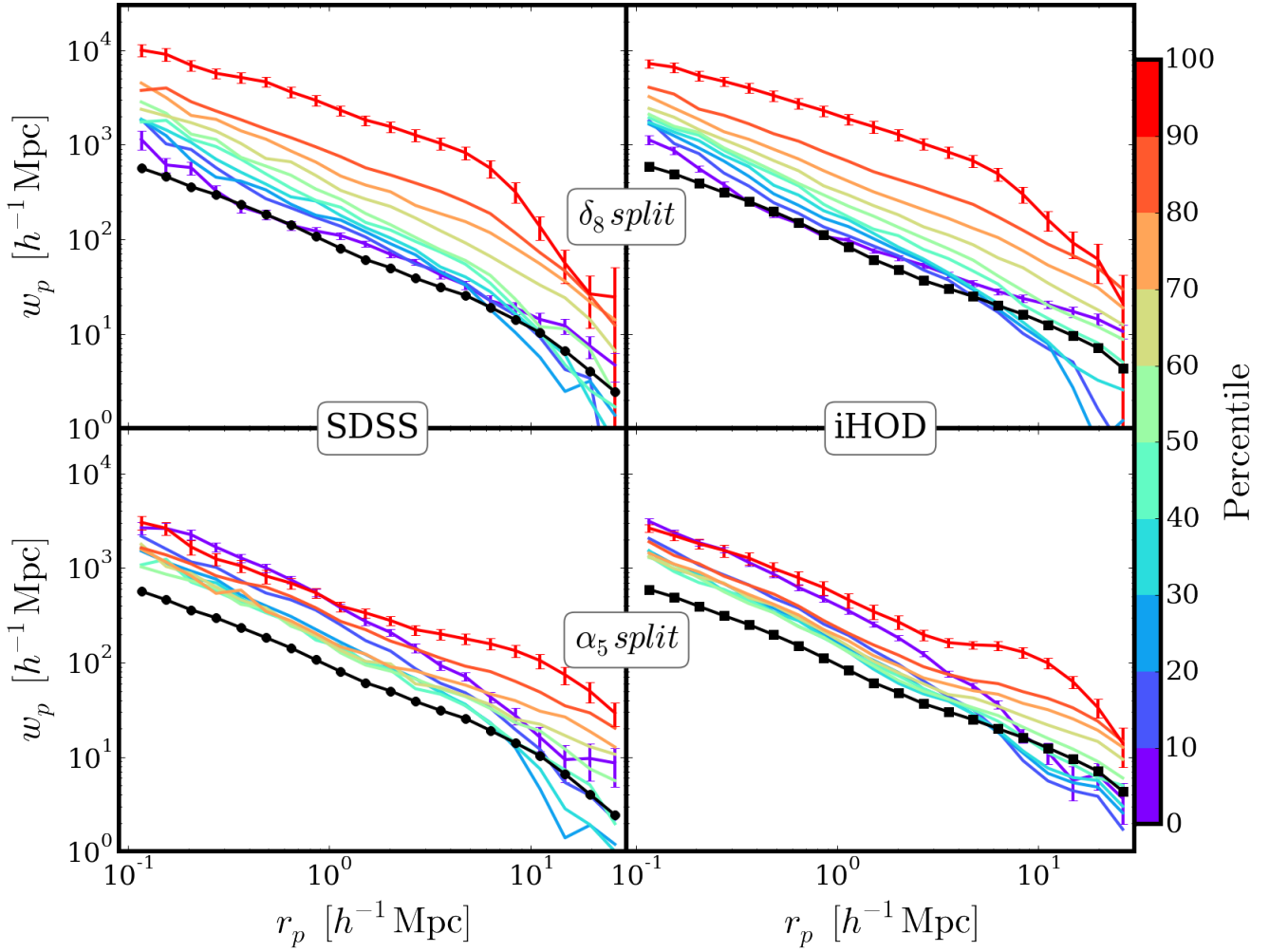


**Figure 3.** The dependence of the projected auto-correlation function  $w_p$  on  $\delta_8$  (top row) and  $\alpha_5$  (bottom row), for the SDSS (left column) and iHOD (right column) galaxies, respectively. In each panel, the black curve shows  $w_p$  for the overall sample and the coloured lines show the auto-correlation  $w_p$  in ten percentile bins of  $\delta_8$  or  $\alpha_5$  as indicated by the colourbar on the right. To avoid clutter, we only show error bars on the overall curve and the top/bottom 10% subsamples in each split. Note that the error bars between different  $r_p$  bins are correlated. This figure shows that  $w_p$  is strong function of both  $\delta_8$  and  $\alpha_5$ , and the behaviour is different at small and large scales.

To minimize the impact due to the small discrepancies in the distributions of  $\delta_8$  and/or  $\alpha_5$  between the SDSS and iHOD catalogues, we always divide galaxies into subsamples based on quantiles instead of fixed bin edges. To further remove the effect due to the residual correlation between the two parameters when splitting galaxies by  $\alpha_5$ , we select fixed quantiles of  $\alpha_5$  at each ten percentile of  $\delta_8$ , and then combine the ten individual  $\alpha_5$  quantiles to form the subsample at that quantile. The errors on  $w_p$  measurements are estimated using 200 jackknife realizations for data and 100 jackknife realizations for the mock catalogue.

Figures 3 & 4 compare the projected auto-correlations and cross-correlations of galaxies split by  $\delta_8$  (top) and  $\alpha_5$  (bottom), between the SDSS (left) and iHOD (right) catalogues, respectively. In each panel, the curves are colour-coded by the ten percentiles marked on the colourbar, ranging from the top 10% (red) to the bottom 10% (purple), while the black circles indicate the  $w_p$  of the overall sample. To avoid clutter, we only show the 1- $\sigma$  measurement uncertainties for the top and bottom 10% subsamples in each panel. Clearly, the projected correlation function of the

SDSS galaxies depends strongly on both  $\delta_8$  and  $\alpha_5$ , and the dependences on small scales are markedly different than on large scales. Note that in general galaxies in regions of high  $\delta_8$  belong to clusters/knots and those with low  $\delta_8$  live in the voids. Galaxies with low  $\alpha_5$  usually reside in isotropic regions which could be either clusters or voids, while those with high  $\alpha_5$  reside in anisotropic tidal environment like sheets and filaments.

When splitting by  $\delta_8$  (top left), on scales below  $r_p \sim 2 h^{-1} \text{Mpc}$  the observed amplitude of  $w_p$  increases monotonically with  $\delta_8$ , while the  $w_p$  shape stays largely unchanged. On scales above  $2 h^{-1} \text{Mpc}$ , however, the amplitude of  $w_p$  becomes a non-monotonic function of  $\delta_8$ , reaching its minimum at the 30 percentile bin. Note that the clustering of the top 10%  $\delta_8$  bin decreases rapidly above  $r_p \sim 8 h^{-1} \text{Mpc}$ , due to the selection effect imprinted by the characteristic scale that we used to define  $\delta_8$ . One key feature of cross-correlations (shown in Figure 4) compared to auto-correlation (shown in Figure 3) is that the clustering signal becomes negative at large scales for low  $\delta_8$  sub-samples because galaxies are residing in under-dense regions, which is

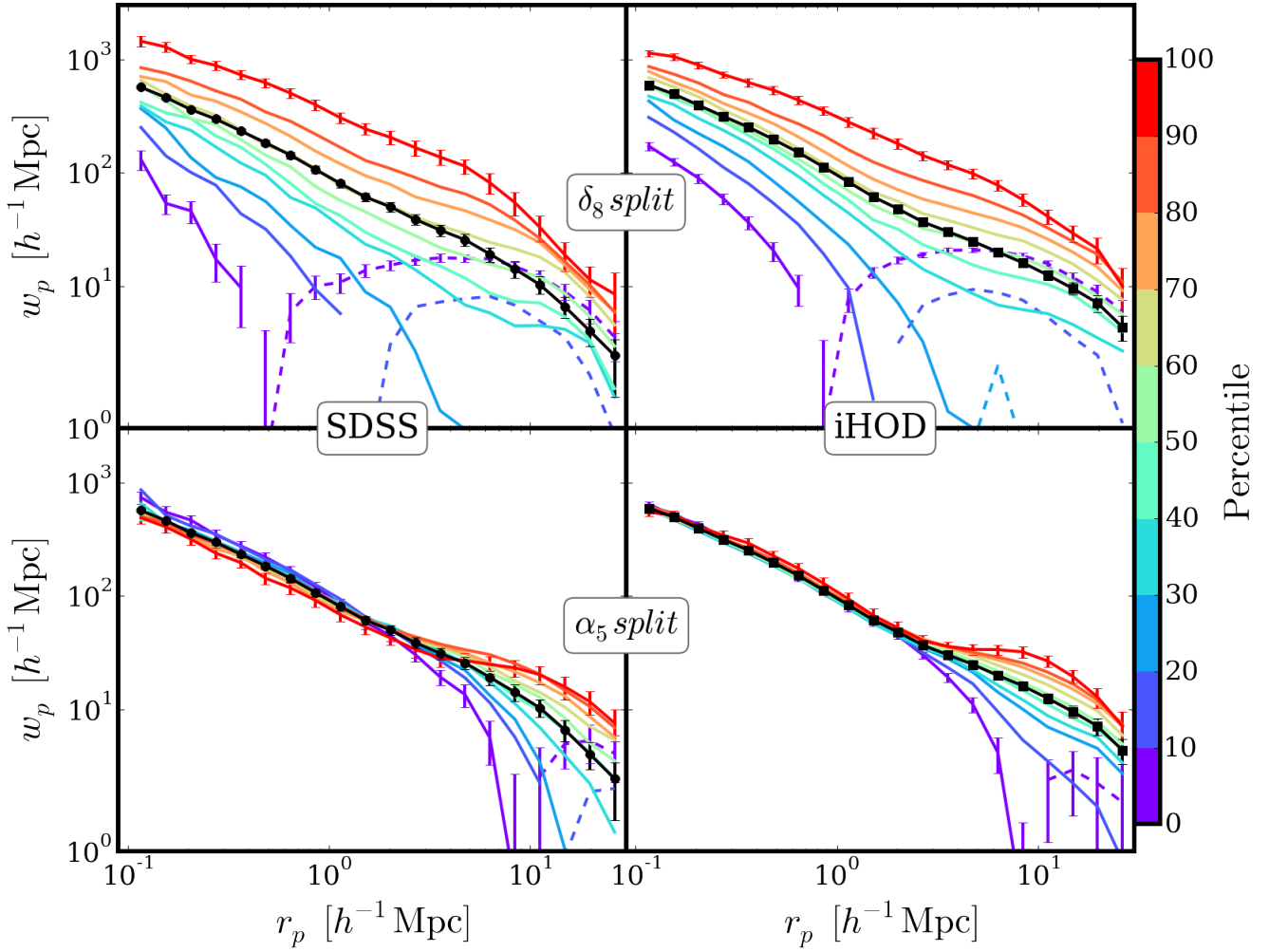


**Figure 4.** The same as Figure 3 but for cross-correlations of galaxies in selected environments with the full sample. The dashed lines indicate negative values where absolute values are plotted. This figure shows that  $w_p$  is negative for low  $\delta_8$  and  $\alpha_5$  at large scales. This also shows that the small scale clustering is independent of  $\alpha_5$  and hence is evidence of the fact that  $\alpha_5$  is independent of  $\delta_8$ .

anti-correlated with the overall density field and hence appears as negatively biased regions. The overall dependence of  $w_p$  on  $\delta_8$  is consistent with the results of Abbas & Sheth (2007). When splitting by  $\alpha_5$  (lower left), the observed  $w_p$  for auto-correlations are non-monotonic functions of  $\alpha_5$  on both small and large scales. In particular, the highest and lowest 10%- $\alpha_5$  subsamples exhibit similar levels of clustering on scales below  $1 h^{-1} \text{Mpc}$ , but their clustering strengths differ by almost a factor of five on scales larger than  $10 h^{-1} \text{Mpc}$ . Note that the measurement of auto-correlation for each subsample is higher than the auto-correlation of the full sample below the smoothing scale used to estimate the environment: this implies that there is a negative cross-correlation between the subsamples (Abbas & Sheth 2007). The observed  $w_p$  for cross-correlations are independent of  $\alpha_5$  at small scales below  $5 h^{-1} \text{Mpc}$ , which is also our smoothing scale for  $\alpha_5$ . But at larger scales they show a strong non-monotonic dependence on  $\alpha_5$ , and the lowest sub-samples of  $\alpha_5$  have negative cross-correlations at large scales (shown with dashed lines in Figure 4).

Such rich and complex phenomenologies in the dependence of  $w_p$  on  $\delta_8$  and  $\alpha_5$ , however, are closely reproduced by the iHOD mock galaxies in the two right panels. Since the apparent cosmic

web dependence of galaxies in the iHOD mock is entirely caused by the variation of halo mass function with large-scale environment, the good agreement between the left and right columns in Figures 3 & 4 suggests that the cosmic web dependence of clustering in the SDSS can be largely explained by an iHOD mock that does not include any galaxy assembly bias, and that any direct impact of the cosmic web on galaxy clustering must be weak in comparison.

To highlight the cosmic web dependence of galaxy clustering in the linear regime, we also measure the large-scale relative bias  $b_{\text{rel}}$  as functions of  $\delta_8$  (left) and  $\alpha_5$  (right), as shown in Figure 5. Throughout the paper, we define the *relative bias* of a subsample as the ratio between the bias of either auto or cross correlations of that subsample and that of the overall sample. The auto- and cross-correlations of subsamples are related to the auto-correlation of all galaxies as follows:

$$w_p^{ss} = b_{\text{rel}}^2 w_p^{\text{aa}} \quad (10)$$

$$w_p^{\text{sa}} = b_{\text{rel}} r_{\text{sa}} w_p^{\text{aa}}, \quad (11)$$

where  $w_p^{\text{aa}}$ ,  $w_p^{\text{sa}}$  and  $w_p^{ss}$  represent the projected correlation functions for all galaxies, cross-correlations of subsamples with all



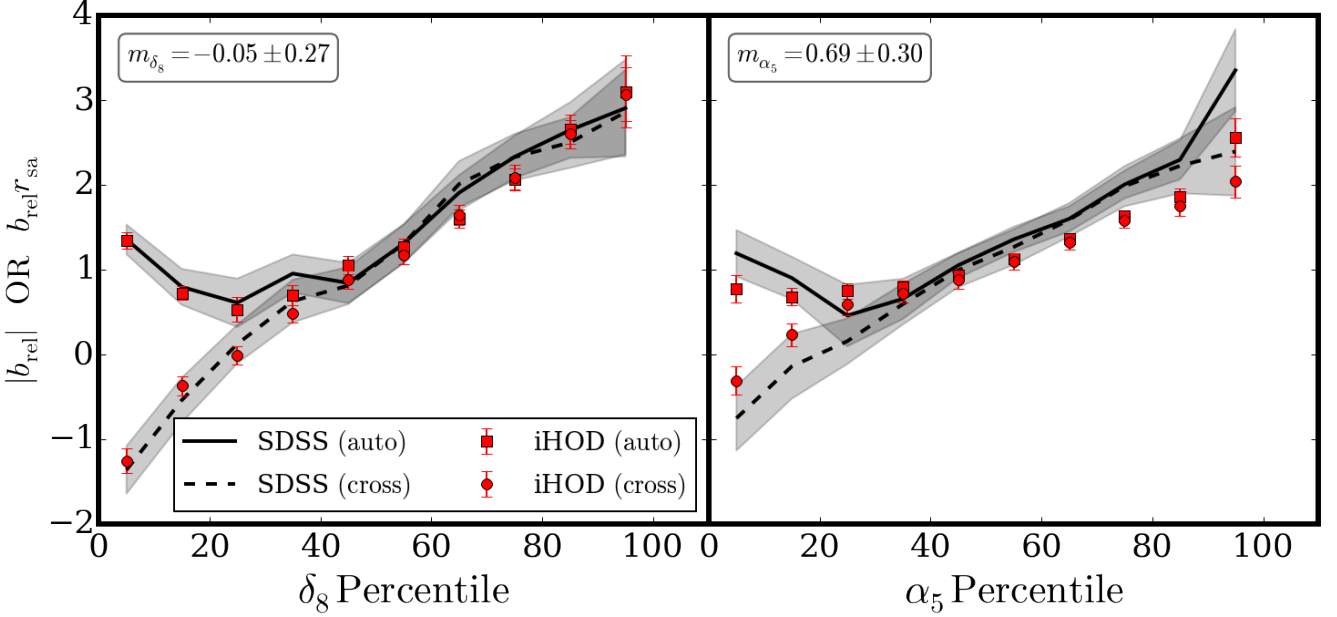


**Figure 5.** The relative bias as a function of  $\delta_8$  (left) or  $\alpha_5$  (right), for the SDSS (black curves with shaded uncertainty bands) and iHOD (red points with error bars) galaxies, respectively. The relative bias of the auto- (cross-)correlation is defined as the ratio between the auto- (cross-)correlation  $w_p$  of each subsample and that of the overall sample, averaged over scales between  $10 h^{-1}\text{Mpc}$  and  $30 h^{-1}\text{Mpc}$ . The errors on the relative bias are estimated using jackknife sampling. Note that the error on the iHOD is smaller due to its larger volume compared to SDSS. The magnitude of the relative bias  $|b_{\text{rel}}|$  shows a characteristic dependence on both  $\delta_8$  and  $\alpha_5$ , which is successfully reproduced by the iHOD model. The auto-correlation is only sensitive to the absolute value of the bias, but the cross-correlation shows that the bias is negative for low values of  $\delta_8$  or  $\alpha_5$ . We also show our linear model constraints on top left corner of each panel, where  $m_{\delta_8}$  and  $m_{\alpha_5}$  are slope parameters of our linear model given in Equation 13 for the two environments respectively.

galaxies and auto-correlations of subsamples, respectively. Note that based on this definition, the auto-correlation measurements only provide the magnitude of relative bias and the cross-correlation measurements reveal the product of the relative bias with the cross-correlation coefficient ( $r_{\text{sa}}$ ). We use jackknife resampling in order to account for the covariance of  $w_p$  between different distance bins including the covariance between the subsample and overall sample. We first estimate the error on the  $w_p$  measurements for the subsample and the overall sample using the variance of jackknife realizations. For each jackknife realization, we estimate the value of relative bias ( $b_{\text{rel}}$ ) corresponding to minimum  $\chi^2$  between projected clustering of a subsample ( $w_p^{\text{sub}}$ ) and overall sample ( $w_p^{\text{aa}}$ ). The  $\chi^2$  is given by the following equation:

$$\chi^2 = \sum_{r_p \geq 10}^{r_p < 30} \left( \frac{w_p^{\text{sub}}(r_p) - b_1 b_2 w_p^{\text{aa}}(r_p)}{\sigma_{w_p}(r_p)} \right)^2, \quad (12)$$

where  $w_p^{\text{sub}}$  represents  $w_p^{\text{ss}}$  for auto-correlation and  $w_p^{\text{sa}}$  for cross-correlations. The diagonal error on  $w_p$  is estimated by adding the error of subsample and overall sample in quadrature (i.e.  $\sigma_{w_p}^2 = \sigma_{w_p^{\text{sub}}}^2 + \sigma_{w_p^{\text{aa}}}^2$ ). For auto-correlations  $b_1 = b_2 = b_{\text{rel}}$  and for cross-correlations  $b_1 = b_{\text{rel}}$  and  $b_2 = r_{\text{sa}}$ . We then compute the mean relative bias and its uncertainty using the bias measurements from all of the jackknife realizations. In each panel, the solid and dashed black line with shaded band indicates the relative bias function and its  $1-\sigma$  uncertainties measured from the auto and cross correlations of SDSS galaxies, while the red squares and circles with error bars are from the iHOD mock galaxies auto and cross correlations respectively. In the left panel, the observed relative bias function from the cross-correlation monotonically increases, with a

zero-crossing around the 20–30 percentile bin and a positive slope. This also shows a characteristic asymmetry where the highest  $\delta_8$  bin has a stronger magnitude of bias compared to the lowest  $\delta_8$  bin. This behaviour of the relative bias can be understood in the context of the peak background split formalism (Kaiser 1984; Sheth & Tormen 1999) as follows: in the initial Gaussian random field, the highest and the lowest  $\delta_8$  regions are equally rare, and therefore should both have similarly high biases. The asymmetry emerged as structures formed non-linearly at later epochs, when the  $\delta_8$  distribution developed a non-Gaussian tail into the high overdensity regime, hence the enhanced magnitude of the bias relative to the underdense regions. The negative sign of the bias for low  $\delta_8$  regions is expected, as the galaxies lying in regions with large-scale density below the mean density will be anti-correlated with the matter field and show negative bias. The auto-correlation function shows essentially the same behaviour except that the auto-correlation is only sensitive to the magnitude of the bias and hence it is positive even in low  $\delta_8$  regions. The amplitude and shape of the observed  $b_{\text{rel}}(\delta_8)$  function are accurately reproduced by the iHOD mock galaxies, indicating that the  $\delta_8$ -dependence of galaxy clustering can be entirely attributed to the overdensity-dependence of the underlying halo mass function. Our findings here for the auto-correlations are consistent with the results of Abbas & Sheth (2007). We also note that the magnitude of the bias from auto-correlations and cross-correlations are very close to each other for all values of  $\delta_8$  and hence the cross-correlation coefficient  $r_{\text{sa}}(\delta_8)$  must be very close to 1 for this sample.

Intriguingly, the observed  $\alpha_5$ -dependence of  $b_{\text{rel}}$  from cross-correlations also exhibits a negative bias in low  $\alpha_5$  bins with an asymmetric magnitude in low- and high- $\alpha_5$  bins in the right panel,

with the zero crossing occurring at the 10–20 percentile of  $\alpha_5$ . Despite the similarities, this  $\alpha_5$ -dependence of the relative bias is independent of  $\delta_8$ , i.e., the large-scale galaxy clustering is an intrinsically strong function of  $\alpha_5$  regardless of  $\delta_8$ , as the conditional probability distributions of  $\delta_8$  are uniform across different  $\alpha_5$  percentiles (by design). The  $\alpha_5$  dependence predicted by the  $\text{iHOD}$  model is qualitatively consistent with the SDSS measurements, except at high  $\alpha_5$  where the predicted relative bias is slightly lower than the observations. In addition, the 1D magnitude of bias in the mock does not rise as significantly as in the data towards the lowest 10% bin, but is nonetheless consistent with the observations within the uncertainties. Similar to  $\delta_8$ , the magnitude of the relative bias from auto-correlations and cross-correlations is very similar as a function of  $\alpha_5$  except in the lowest and highest bins, and hence the cross-correlation coefficient  $r_{\text{sa}}(\alpha_5)$  must be very close to 1 for this sample except for extreme values of  $\alpha_5$  for both SDSS and  $\text{iHOD}$ .

It is interesting to consider the formal degree of agreement between the above measurements and the  $\text{iHOD}$  predictions. This can be addressed directly by using our jackknife realizations to estimate the covariance matrix for the bias data. Considering both the auto- and cross-correlation estimates together, we can evaluate  $\chi^2$  on 20 degrees of freedom. The  $\delta_8$  measurements yield  $\chi^2 = 8.4$ , which is statistically acceptable; the  $\alpha_5$  results agree less well visually but statistically give  $\chi^2 = 25.2$  – corresponding to a  $p$ -value of 20%. If one regards the current outcome as a null result, it is interesting to ask what level of effect could be clearly detected by an analysis of this sort. As an illustrative answer to this question, we have considered an empirical linear model for the relation between relative bias and environment:

$$b_{\text{rel}}^{\text{SDSS}}(\text{env})r_{\text{env}} = b_{\text{rel}}^{\text{iHOD}}(\text{env})r_{\text{env}} + m_{\text{env}}R_{\text{env}} + c_{\text{env}}, \quad (13)$$

where  $\text{env}$  is either  $\delta_8$  or  $\alpha_5$  with  $m_{\text{env}}$  and  $c_{\text{env}}$  are the two parameters of our model accounting for any systematic difference between SDSS and  $\text{iHOD}$ . Here,  $R_{\text{env}}$  represents the rank of  $\text{env}$  bins mapped to the interval  $[-0.5, 0.5]$ . In this model,  $b$  means the bias with definite sign inferred from cross-correlation, so it is not a linear model for  $|b|$ . This means for auto-correlations  $r_{\text{env}}$  is set to +1 for bins above 20–30 percentile and –1 for lower percentile bins whereas for cross-correlations we directly measure the product  $b_{\text{rel}}r_{\text{env}}$ . We ran an MCMC analysis to estimate  $m_{\text{env}}$  after marginalizing over  $c_{\text{env}}$  and accounting for covariances in the measurement of relative bias using the jackknife. The results show that  $m_{\alpha_5}$  can be constrained with an rms error of 0.30, so that effects with slopes above about 1 could have been clearly detected if they had been present. We also found that for  $\text{iHOD}$  the  $m_{\alpha_5} = 0.69 \pm 0.30$  which is  $2.3\sigma$  deviation. It is a matter of debate whether this degree of mismatch should be taken as evidence for a physical effect of the cosmic web environment, or whether it might indicate a small imprecision in the  $\text{iHOD}$  mocks. For example, our measurements are made in redshift space and are thus sensitive in particular to the exact amplitude of Finger-of-God virialized velocities. We have used N-body simulations to study the impact of peculiar velocity on such measurements and found that a similar deviation in  $m_{\alpha_5}$  can be produced when the peculiar velocities of galaxies are scaled by a factor of 3. Exploring marginalization over such effects is beyond the scope of this work, but because of the outcome of this simple peculiar velocity study, we do not currently claim any strong evidence for detection of direct tidal effects of the cosmic web. We have also measured  $m_{\delta_8} = -0.05 \pm 0.27$ , which is statistically consistent with zero. So, if one considers both  $m_{\alpha_5}$

and  $m_{\delta_8}$  together then we find no strong evidence for a deviation between SDSS and  $\text{iHOD}$  using this simple linear model.

To better understand the origin of the strong dependence of  $|b_{\text{rel}}|$  with  $\alpha_5$  in both the data and mock catalogues, we can examine the relative bias as a 2D function of both variables simultaneously, by calculating the projected auto-correlation functions of subsamples defined on the  $\delta_8$  vs.  $\alpha_5$  plane. Figure 6 compares this 2D bias function measured from SDSS (left) to that from the  $\text{iHOD}$  mock (right). In each panel, the colour-coding indicates the value of the relative bias in each cell of  $(\alpha_5, \delta_8)$ , with the colour bar shown on the right. The numbers displayed in each cell shows the errors on the relative bias of the cell. Similarly Figure 7 shows the 2D bias function but measured using cross-correlations. It is clear that the observed galaxy bias depends on both  $\alpha_5$  and  $\delta_8$  simultaneously, and the 2D bias map shows several interesting features on the  $\alpha_5$  vs.  $\delta_8$  plane:

- The low-bias galaxies live predominantly in under-dense regions (bottom 50%  $\delta_8$ ), but at each fixed  $\delta_8$  percentile, the lowest magnitude of bias occurs at different percentiles of  $\alpha_5$  — galaxies with high  $\alpha_5$  and low  $\delta_8$  have a similar bias to those with low  $\alpha_5$  and intermediate  $\delta_8$ .
- Galaxies that live inside the densest portion of the filaments (high- $\delta_8$  and high- $\alpha_5$ ; top right corner) have the strongest large-scale clustering bias.
- Galaxies that live in isolated voids (low- $\delta_8$  and low- $\alpha_5$ ; bottom left corner) have a relatively strong bias compared to those in the field but with negative sign.
- Galaxies that live in the most isolated and densest knots (top 10%  $\delta_8$  and bottom 10%  $\alpha_5$ ; top left corner) have a relatively low bias, reflecting the rapid decline of  $w_p$  on scales above  $8 h^{-1} \text{Mpc}$  (see the red curve in the top left panel of Figure 3).

Moreover, we can better understand the dependences of the 1D relative bias (seen in Figure 5) by averaging the 2D bias map along each of the two axes. Specifically, the strongest 1D bias at the high  $\alpha_5$  or high  $\delta_8$  end is contributed solely by galaxies inside the dense filaments, while the enhanced 1D bias at the bottom 10% of  $\alpha_5$  or  $\delta_8$  is caused by galaxies inside the isolated voids. The minimum 1D bias occurs at the 20–30 percentile of  $\alpha_5$  or  $\delta_8$ , primarily due to the lack of any such galaxies living in dense filaments or isolated voids.

Naively, the dependence on  $\alpha_5$  seen in the left-hand panel of Figures 6 and 7 might lead us to conclude that galaxy clustering is indeed directly influenced by tidal forces within the cosmic web. In particular, to model the clustering of any stellar mass (or luminosity) limited galaxy sample, one usually assume a uniform HOD for that sample across all types of cosmic web environment. For example, the mean central galaxy occupation can be described as

$$\langle N_{\text{cen}} \rangle (M_h) = \frac{1}{2} \left[ 1 - \text{erf} \left( \frac{\log M_h - \log M_{\text{min}}}{\sigma_{\log M_h}} \right) \right], \quad (14)$$

where  $M_{\text{min}}$  corresponds to the halo mass scale that yields  $\langle N_{\text{cen}} \rangle = 0.5$ , while  $\sigma_{\log M_h}$  controls the sharpness of the transition from  $\langle N_{\text{cen}} \rangle = 0$  to 1 (Zheng et al. 2005). However, it is plausible that  $M_{\text{min}}$  and  $\sigma_{\log M_h}$  are both functions of  $\delta_8$  and/or  $\alpha_5$  (see McEwen & Weinberg 2016; Wibking et al. 2017, for an interesting example of a  $\delta_8$ -dependent HOD). For instance, to boost the clustering of galaxies with high  $\delta_8$  and  $\alpha_5$ , one could make  $M_{\text{min}}$  larger and/or  $\sigma_{\log M_h}$  smaller in the dense filamentary environments than in the field.

If the HOD indeed depends strongly on the cosmic web, one would expect that the  $\text{iHOD}$  mock galaxies are unable to reproduce

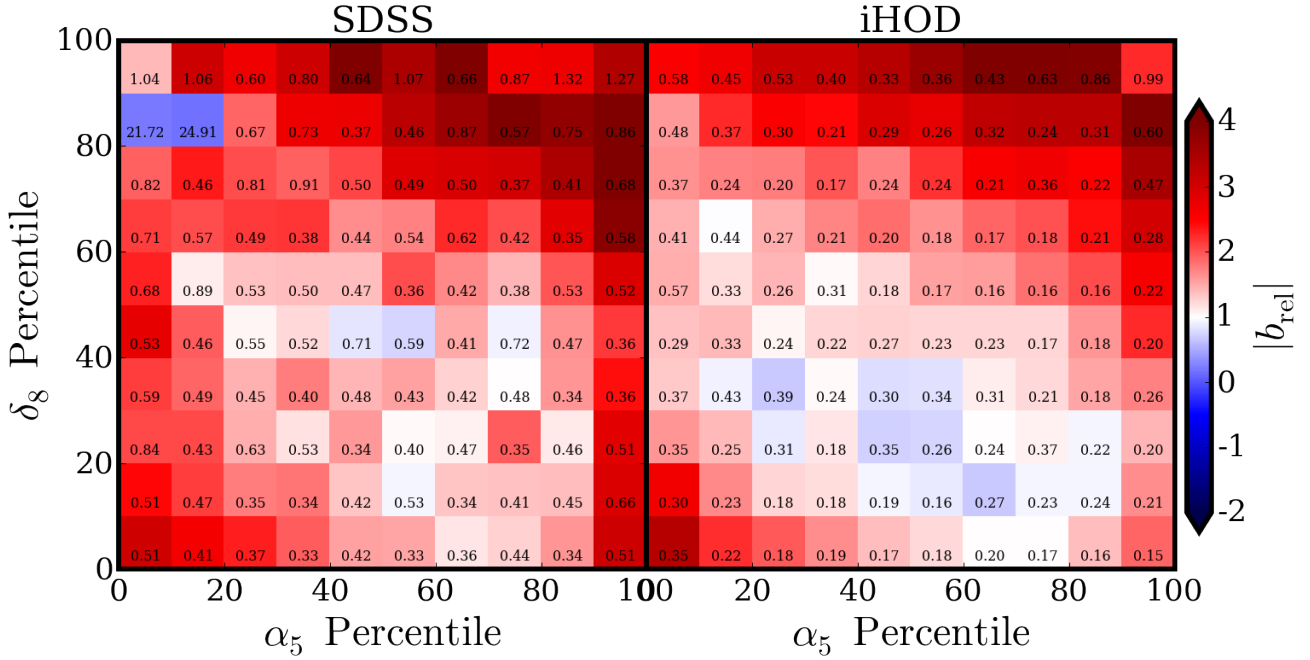


**Figure 6.** Comparison of the relative biases between the SDSS (left) and iHOD (right) galaxies on the  $\delta_8$ - $\alpha_5$  plane. Each cell is colour-coded by the bias relative to the overall sample of galaxies in a 2D bin of ten percentile in  $\delta_8$  and  $\alpha_5$  jointly. The numbers displayed in each cell show the statistical errors on the relative bias of the corresponding cell.

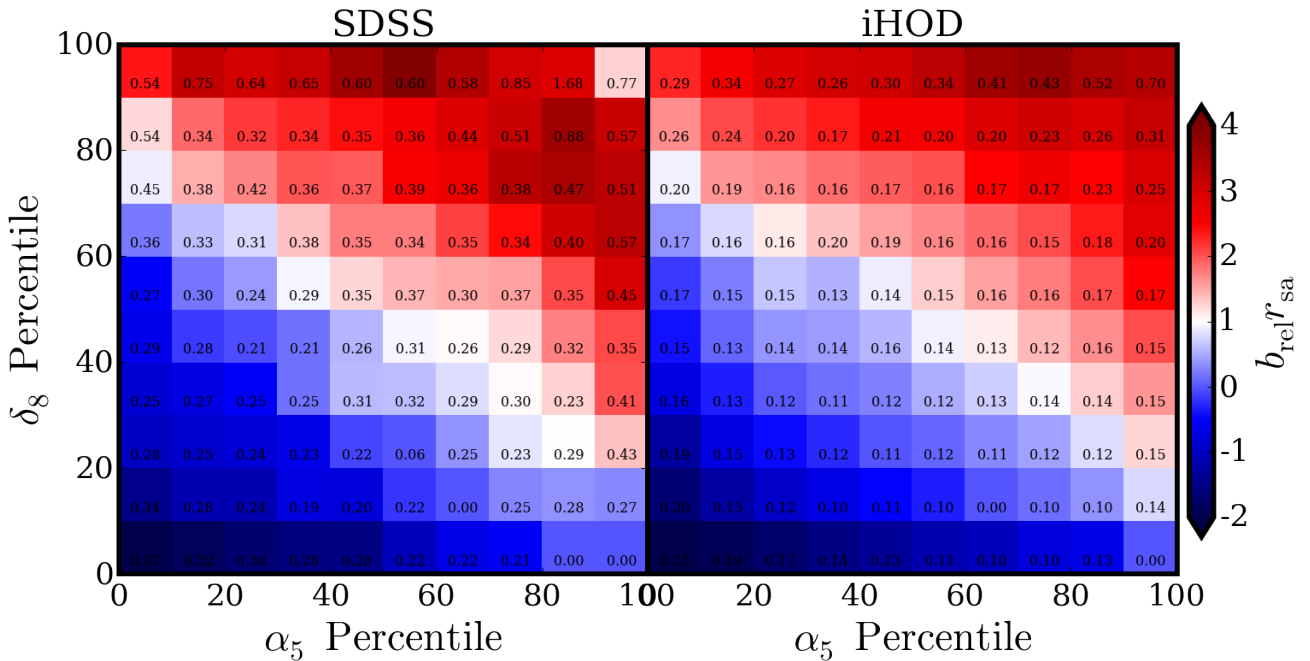


**Figure 7.** Similar to Figure 6 but using cross-correlation to measure relative bias.

the observed 2D bias map from SDSS, because the mock catalogue does not include any dependence on  $\delta_8$  or  $\alpha_5$ . However, the mock 2D bias map shown in the right panel provides a good match to the observations on the left, qualitatively reproducing all the features discussed above. The mock bias varies slightly more continuously across adjacent cells than the observed bias due to the better statistics (i.e., larger volume) in the mock. There are some discrep-

ancies between the observed and the mock bias maps within the  $\alpha_5$  range between 0 and 20 percentiles, echoing the lack of an enhanced bias at the lowest  $\alpha_5$  end in the mock (see the right panel of Figure 5). However, it is unclear whether such discrepancies reflect the shortcomings of the iHOD model in describing the clustering of galaxies in the extremely low  $\alpha_5$  regime, or merely statistical fluctuations that will vanish in future larger surveys. We will inves-

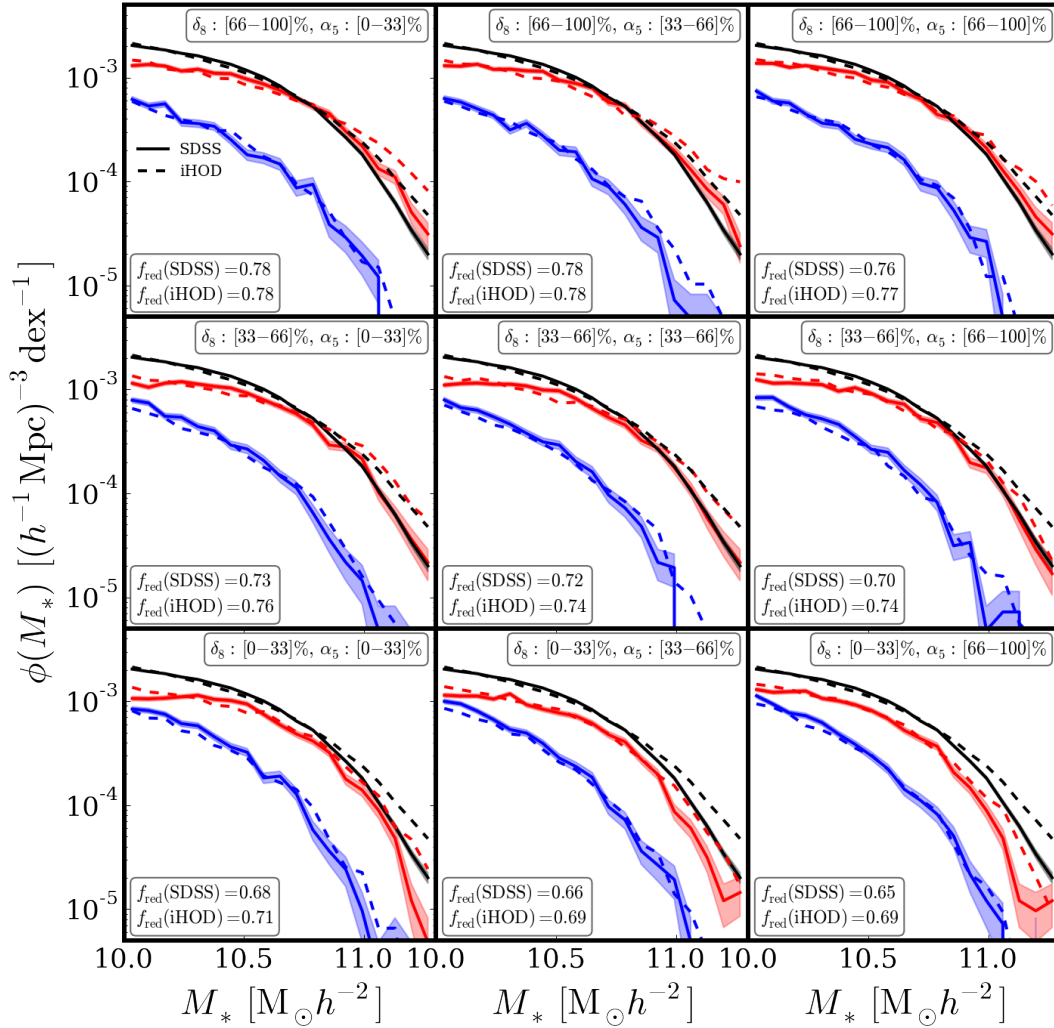


**Figure 8.** Stellar mass functions of red and blue galaxies in 2D bins of  $\delta_8$  and  $\alpha_5$  (from top to bottom rows: top, middle, and bottom 1/3 in  $\delta_8$ ; from left to right columns: top, middle, and bottom 1/3 in  $\alpha_5$ ; see the top right legend), for SDSS (solid curves with shaded uncertainty bands) and iHOD (dashed curves) samples, respectively. In each panel for each sample, the black, red, and blue curves indicate the overall, red, and blue galaxies, respectively, with the overall curve normalized to have 1/9 of the total number density in each sample. The red galaxy fractions in each 2D bin are listed in the bottom left corner of each panel. The remarkable agreement of SDSS and iHOD in this figure suggests that observed relative abundances of red and blue galaxies do not require any additional cosmic web dependence on top of what is produced through halo mass.

tigate the sources of those discrepancies in more detail in a future paper (Salcedo et al, in prep.).

Overall, there is good agreement between the data and the iHOD mock in describing the cosmic web dependence of galaxy clustering on all scales, as shown by the combination of Figures 3–7. The only place where iHOD appears to fail slightly is in predicting the  $\alpha$ -bias relation to be a little weaker compared to SDSS data as shown in Figure 5. This is encouraging, suggesting that the additional dependence of HOD on the cosmic web is small, as the observed trend of galaxy bias with cosmic web properties can be largely described by the inherent dependence of halo mass function on those properties encoded in the iHOD model.

#### 4.2 Dependence of galaxy quenching on $\delta_8$ and $\alpha_5$

We have shown in the above section that, before splitting by any quenching properties, galaxy occupation statistics seem to be a weak function of the cosmic web environment. However, it is plau-

sible that the quenching of galaxies is influenced by the cosmic web despite the fact that the overall galaxy formation efficiency is largely independent of  $\delta_8$  and  $\alpha_5$ . For example, the halo gas accretion could be heavily regulated by the tidal anisotropy, so that it is easier for streams of cold gas to penetrate halo boundaries if they were funnelled through the filaments than in an isotropic tensor environment, where the ‘hot mode’ accretion usually takes over (Kereš et al. 2005). Therefore, if the quenching of star formation is primarily caused by the shutdown of cold gas accretion, rather than the removal of the gas reservoir and/or the heating of gas (through various feedbacks and virial shocks), we would expect a strong cosmic web dependence of galaxy quenching.

To investigate whether a strong cosmic web quenching exists, we divide the observed galaxies into quenched vs. star-forming according to their  $g-r$  colours, and measure the relative abundance and clustering bias of red (quenched) vs. blue (star-forming) galaxies in different cosmic web environments defined by  $\delta_8$  and  $\alpha_5$ . Following a similar route as in § 4.1, we perform the same analysis



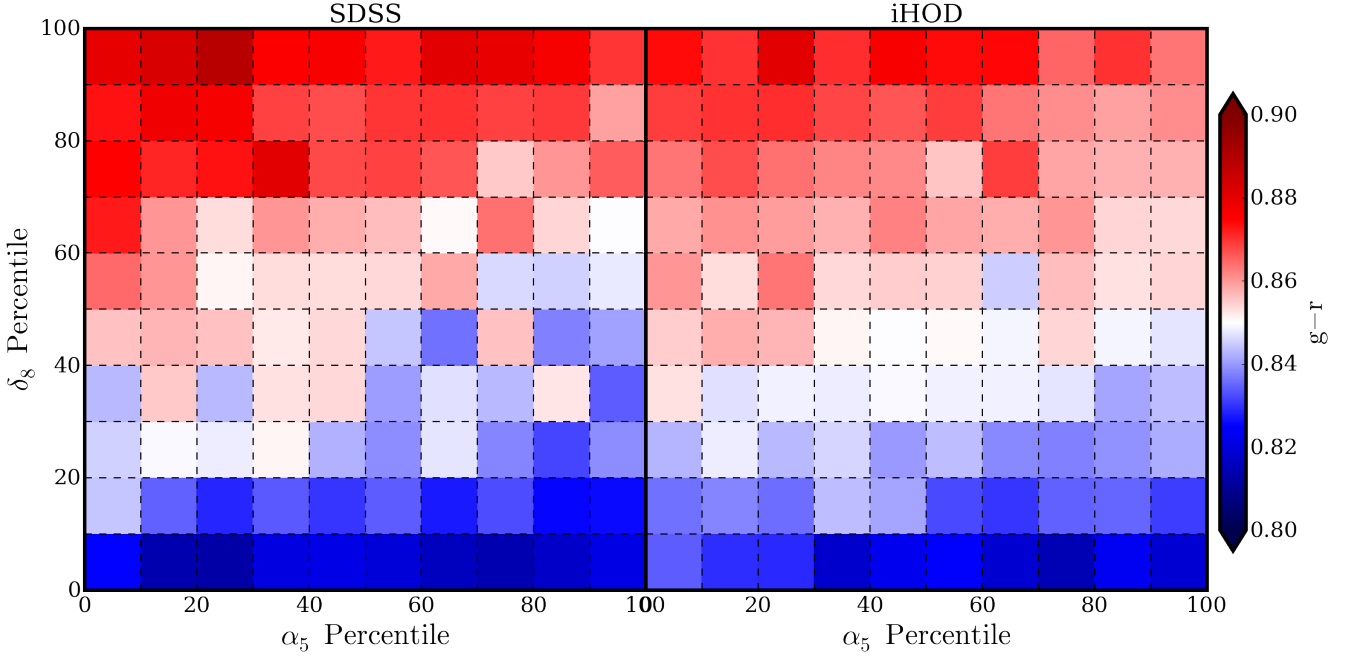


**Figure 9.** Similar to Figure 6, but for the mean  $g-r$  colour of galaxies. The figure shows that the mean  $g-r$  colour depends both on  $\delta_8$  and  $\alpha_5$  in both SDSS and iHOD. The subtle dependence of mean  $g-r$  colour on  $\alpha_5$  is unlikely to be the evidence of tidal dependence of galaxy quenching because it is reproduced by the iHOD model, which does not include any such effect.

over the iHOD mock galaxies and compare with the SDSS measurements, in hopes of detecting any cosmic web dependence of galaxy quenching that is absent from the fiducial halo quenching model of Zu & Mandelbaum (2017).

To separate galaxies into red and blue, we use the stellar mass dependent colour split as suggested in equation 2 of Zu & Mandelbaum (2016). We first compare the relative abundances of red vs. blue galaxies between SDSS and iHOD across various cosmic web environments, as shown in Figure 8. Within each catalogue, we divide galaxies into nine subsamples based on their  $\delta_8$  and  $\alpha_5$  percentiles, indicated by the legend on the top right of each panel. In each panel, we show the red (red curves) and blue (blue curves) galaxy stellar mass functions for the SDSS (solid) and iHOD (dashed) galaxies, respectively. The red galaxy fractions of the SDSS and iHOD subsamples are also listed in the bottom left of each panel. We show the jackknife  $1-\sigma$  uncertainties of the SDSS abundances as shaded bands, while the uncertainties for the iHOD measurements are much smaller due to better statistics (not shown here to avoid clutter).

Uniform across all panels, the black solid and dashed curves indicate the overall stellar mass functions (SMFs; reduced by a factor of nine for easy comparison) of the SDSS and iHOD galaxies, respectively. The overall SMF of the iHOD galaxies agrees very well with that of the SDSS galaxies at  $M_* < 10^{11} h^{-2} M_\odot$ . As emphasized in Zu & Mandelbaum (2015), this agreement of overall SMFs is not by construction, as the SMF is a prediction from the best-fitting iHOD model, rather than an input to the constraint. The iHOD SMF has a slightly higher amplitude than the observed one at the extreme high mass end, probably induced by a combination of observational and model systematics. Fortunately, our statistical results are dominated by galaxies with  $M_* < 10^{11} h^{-2} M_\odot$ , and are thus robust to any SMF discrepancy at the very high mass regime.

The relative abundance of red vs. blue galaxies exhibits strong

dependence on  $\delta_8$  in the SDSS, with the red galaxy fraction  $f_{\text{red}}$  increasing from  $\sim 68\%$  at low  $\delta_8$  (bottom row) to  $\sim 78\%$  at high  $\delta_8$  (top row), regardless of  $\alpha_5$ . This  $f_{\text{red}}-\delta_8$  relation is expected from the well-known colour-density relation (Oemler 1974; Davis & Geller 1976; Dressler 1980). At fixed  $\delta_8$ , however, the observed relative abundance of red vs. blue galaxies shows little variation with  $\alpha_5$ . The cosmic web dependence of the colour-split SMFs predicted by the iHOD mock shows excellent agreement with that observed in the SDSS, with the dashed curves closely tracking the solid ones in each panel. Such high level of agreement is remarkable, because the colour-split SMFs in the iHOD model are predicted from the fiducial halo quenching model, which is constrained solely by the spatial clustering and weak lensing of the red vs. blue galaxies in SDSS. Since the cosmic web dependences of the colour-split SMFs in the iHOD mock are entirely inherited from the cosmic web dependence of the halo mass functions via halo quenching, this agreement suggests that no cosmic web quenching is required to reproduce the observed relative abundance of red vs. blue galaxies across different cosmic web environments.

An alternative quantity for statistically characterizing the quenched level of a galaxy sample is the average colour of that sample  $\langle g-r \rangle$ , which has the advantage of not relying on a somewhat arbitrary colour split to divide galaxies into red and blue. The disadvantage is that the mock galaxy colours, if predicted by semi-analytic models or hydrodynamic simulations, usually have difficulties reproducing the observed colour distributions to very high precision (Henriques et al. 2015; Sales et al. 2015; Bray et al. 2016). However, thanks to the colour assignment scheme implemented in Zu & Mandelbaum (2017), at any fixed  $M_*$  the mock colours follow a double-Gaussian distribution that is inferred from a volume-limited sample in the SDSS. Therefore, we can directly compare the cosmic web dependence of  $\langle g-r \rangle$  predicted by the iHOD halo quenching model to that observed in the SDSS.

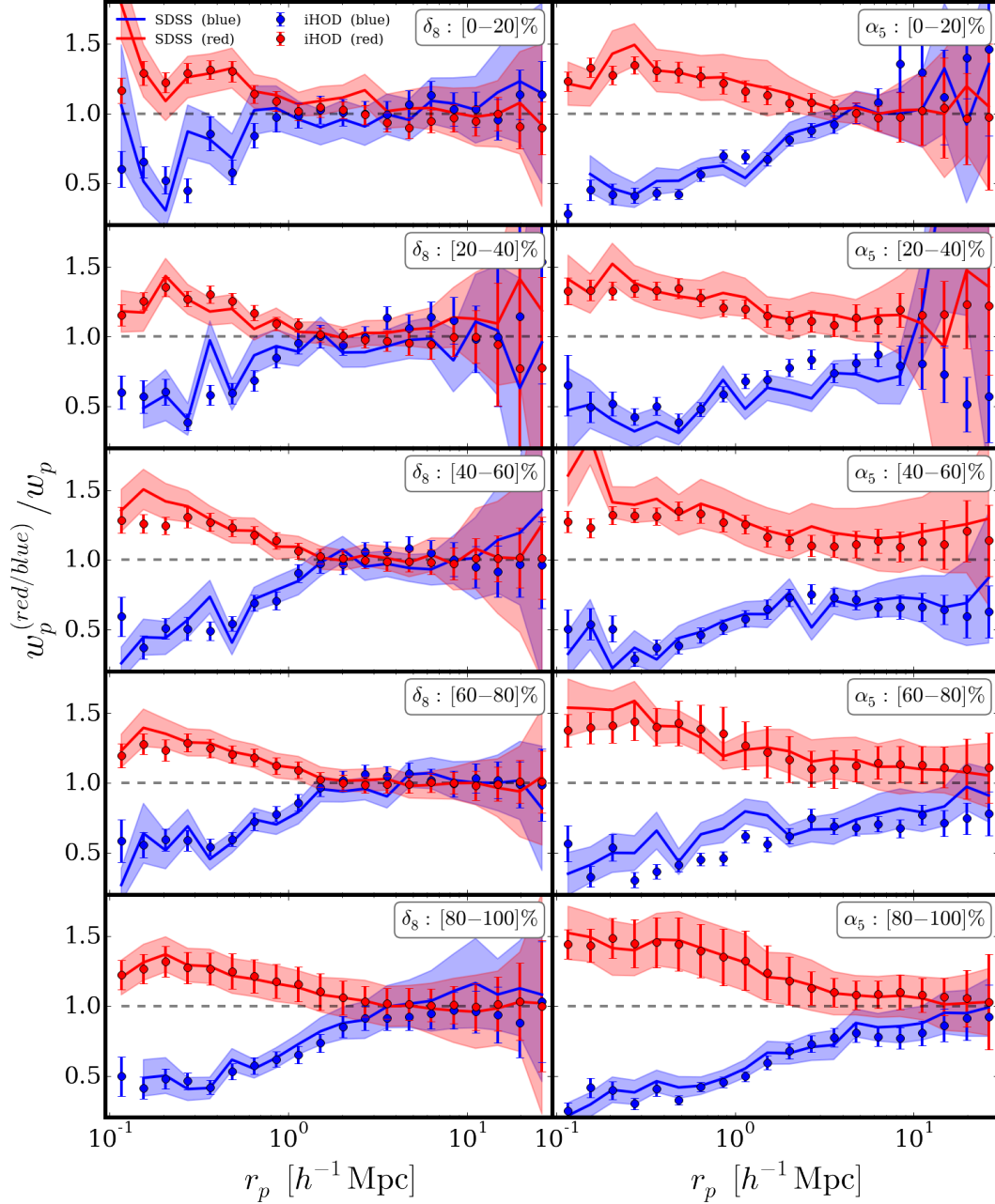


**Figure 10.** The relative clustering of the galaxies in each coloured subsample to that of the overall sample in 20 percentile bins of  $\delta_8$  (left) and  $\alpha_5$  (right), respectively. In each panel, solid curves with shaded  $1\text{-}\sigma$  uncertainty bands indicate the SDSS galaxies, and the circles with error bars show results for the  $\text{iHOD}$  galaxies. The relative clustering of each red (blue) subsample is defined as the projected cross-correlation of red (blue) subsample and the overall sample within that 2D bin, divided by the projected auto-correlation of the overall sample. The two key results shown in this figure are that the characteristic scale at which red and blue galaxies have the same clustering depends on environment and the large scale relative bias of red and blue galaxies are the same in all  $\delta_8$  bins but differ from each other in some  $\alpha_5$  bins.

We compute  $\langle g-r \rangle$  as a 2D function of  $\delta_8$  and  $\alpha_5$ , using the same subsamples defined earlier for the 2D relative bias comparison. Figure 9 shows the result for the SDSS galaxies on the left and  $\text{iHOD}$  mock on the right. The mean  $g-r$  colour of the full  $\text{iHOD}$  catalogue is the same as that in the SDSS (0.85; shown as white colour on the 2D colour map). Consistent with our findings in Figure 8, the average colour depends primarily on  $\delta_8$  in both catalogues, with the reddest (bluest) population living in regions with the top (bottom) 10%  $\delta_8$ . However, the left panel of Figure 9

reveals a subtle  $\alpha_5$  dependence that was indiscernible in Figure 8 — at fixed narrow range of  $\delta_8$ , galaxies that live in high- $\alpha_5$  regions appear to be slightly bluer than those live in low- $\alpha_5$  regions. Note that this  $\alpha_5$  dependence reflects an overall reduction in the quenched fraction, rather than any relative decrease of the high- $M_*$  (thus redder) galaxies in high- $\alpha_5$  environments (which is not seen in Figure 8).

One might think that the physical cause of this subtle  $\alpha_5$  dependence is related to the impact of tidal anisotropies on galaxy

quenching. However, in the right panel of Figure 9, the cosmic web dependence of the mean colour predicted by the fiducial halo quenching model shows very good consistency with the observations on the left, including both the strong  $\delta_8$  dependence and the subtle variation with  $\alpha_5$ . As a result, this agreement shown in Figure 9 between SDSS and  $\mathbf{iHOD}$  suggests that this intriguing  $\alpha_5$ -dependence of  $\langle g-r \rangle$  is unlikely to be evidence of direct tidal impact on galaxy quenching, but is again an imprint left by halo quenching via the cosmic web modulation of halo mass function.

A similar dependence of mean colour on tidal environment was found by Yan et al. (2013) (see their Figures 3 & 4). They showed that such a dependence was mostly due to the choice of smoothing scale, and that it will disappear if one uses an adaptive smoothing that maximizes the density-colour relation. We have also looked at the effect of smoothing scale on our mean colour with over-density and tidal anisotropy. We found that using a different smoothing scale does not affect the mean colour for regions with over-density below the 50th percentile. We observed that as we reduce our smoothing scale, the colour of high over-density and low tidal anisotropy (top left part) reduces at the same time as the mean colour of high over-density and high tidal anisotropy (top right) increases. This might happen because we are working in apparent redshift space and hence while using smaller smoothing we become more sensitive to the distortion in density introduced by peculiar velocity. Hence, clusters (which should have an isotropic tidal environment) appear more and more anisotropic (filamentary), leading to a high value of  $\alpha$ . Therefore if one is working in apparent redshift space it will be important for the mocks to reproduce the peculiar velocity of galaxies, in order to match such colour distributions for smaller smoothing scales.

Finally, we examine the relative clustering of red vs. blue galaxies as a function of  $\delta_8$  (left) and of  $\alpha_5$  (right) in Figure 10. In each column, we divide galaxies in each of the two catalogues into five equal-size bins according to their  $\delta_8$  or  $\alpha_5$ . In each 20 percentile bin, we compute the relative clustering of a coloured sample as the ratio of  $w_p^{\text{color}}$  and  $w_p$ , where  $w_p^{\text{color}}$  is the cross-correlation between the red/blue galaxies and all galaxies in that bin, and  $w_p$  is the auto-correlation of all galaxies in that bin. In each panel, solid curves with shaded bands are the SDSS measurements and 1- $\sigma$  uncertainties, while the solid circles with error bars are from the  $\mathbf{iHOD}$  mock.

At fixed  $\delta_8$  (left panels), the red and blue SDSS galaxies show very similar clustering biases on large scales. This can be understood by examining Figure 6, 8, and 9 simultaneously — although the large-scale bias varies with  $\alpha_5$  at fixed  $\delta_8$ , the red galaxy fraction and average galaxy colour vary much less so with  $\alpha_5$ , indicating that the red and blue galaxies are not segregated into regions of different biases. However, the clustering amplitudes of the red and blue galaxies exhibit strong discrepancies on small scales, and the characteristic scale at which the two start deviating increases monotonically with  $\delta_8$ , from  $\sim 0.6 h^{-1}\text{Mpc}$  (top left) to  $3 h^{-1}\text{Mpc}$  (bottom left). In the lowest  $\delta_8$  bin, this characteristic quenching scale roughly corresponds to the size of the most massive haloes in that under-dense environment, whereas in the highest  $\delta_8$  bin it grows much larger than the size of a single massive halo. The large characteristic quenching scale in dense regions is consistent with the so-called ‘2-halo conformity’ phenomenon (Kauffmann et al. 2013), i.e., the coherent quenching of galaxies within the same large-scale overdensity environment. However, the relative clustering of the red vs. blue galaxies predicted by the  $\mathbf{iHOD}$  halo quenching model (solid circles) is in excellent agreement with the measurements from SDSS in all  $\delta_8$  environments, including

the small-scale discrepancy between the clustering amplitudes of the two colours, as well as the characteristic quenching scale as a function of  $\delta_8$ . This agreement echoes the findings in Zu & Mandelbaum (2017), that the observed 2-halo conformity effect can be largely explained by the simple halo quenching, mediated by the environmental dependence of halo mass functions (see also Tinker et al. 2017; Sin et al. 2017; Calderon et al. 2017).

Although we have seen that red and blue galaxies have identical large-scale bias when considering subsamples at constant  $\delta_8$  this is not the case when we split by  $\alpha_5$ . In the right-hand panels of Figure 10, we see that the red SDSS galaxies exhibit stronger large-scale clustering bias than the blue ones at high  $\alpha_5$  (bottom three panels on the right), but have a comparable bias at low  $\alpha_5$  (top two panels on the right). This finding can be understood as follows. Figure 6 shows that the large-scale bias increases monotonically with  $\delta_8$  at high  $\alpha_5$ , while according to Figure 9 the galaxies are progressively more quenched at higher  $\delta_8$  at any fixed  $\alpha_5$ . Therefore, we expect the red galaxies to have a stronger large-scale bias than the blue ones at high  $\alpha_5$ . However, the large-scale bias changes non-monotonically with increasing  $\delta_8$  at low  $\alpha_5$ , so that the low and high- $\delta_8$  galaxies have comparable large-scale biases (see Figure 6). By the same token, we expect the bias-colour trend to be reversed at low  $\alpha_5$  and that the blue galaxies have a similar large-scale bias as the red ones. On scales below  $5 h^{-1}\text{Mpc}$ , the red galaxies clustered more strongly than the blue ones across all  $\alpha_5$  environments. Similar to the left panels, the observed  $\alpha_5$  and scale dependences of the relative clustering of two colours are closely reproduced by the predictions from the  $\mathbf{iHOD}$  quenching model.

The combination of Figures 8, 9 & 10 demonstrates that, although the observed galaxy quenching properties (including the relative abundance and clustering of the red vs. blue galaxies) have a complicated apparent dependence on cosmic web, those dependences can be entirely explained by the fiducial halo quenching model in  $\mathbf{iHOD}$ , constrained solely by the spatial clustering and the weak lensing of red and blue galaxies in the SDSS. The surprising success of such a simple quenching model, described by merely four parameters, strongly suggests that the galaxy quenching process is primarily driven by halo mass, and the large-scale ( $> 5 h^{-1}\text{Mpc}$ ) tidal environment has little direct influence on the colour transformation of galaxies above  $10^{10} h^{-2} M_\odot$ .

## 5 SUMMARY AND DISCUSSION

We have measured the dependence of galaxy clustering and quenching on the cosmic web properties in the SDSS, characterized by the combination of galaxy overdensity ( $\delta_8$ ) and tidal anisotropy ( $\alpha_5$ ) at each galaxy position. We have developed an improved method to measure the tidal tensor field from the observed galaxy distribution in redshift surveys, by applying more accurate density estimation scheme using tessellations. We always work with the apparent redshift-space tidal field estimated using exactly same method for SDSS galaxies and mock galaxies. In order to reveal any *direct* cosmic web effect on galaxy formation, we compare the observed dependences in the SDSS to those measured from an HOD galaxy mock catalogue built from the  $\mathbf{iHOD}$  fiducial halo quenching model of Zu & Mandelbaum (2015, 2016, 2017). The galaxy-cosmic web relation in the  $\mathbf{iHOD}$  mock is solely derived from the cosmic web modulation of the underlying halo mass function, as the stellar mass, occupation statistics, and optical colour of the mock galaxies are determined only by the mass of the host haloes.

The projected correlation function ( $w_p$ ) of galaxies shows complicated  $\delta_8$  and  $\alpha_5$  dependences on both the small and large scales. In particular, the large-scale clustering bias of galaxies exhibits a characteristic dependence on  $\delta_8$  as well as  $\alpha_5$ , with the 1D bias functions having their lowest absolute values around the 30 percentile of  $\delta_8$  and  $\alpha_5$ , respectively. We investigated the origin of such characteristic dependences by examining the 2D galaxy bias function on the  $\delta_8$ - $\alpha_5$  diagram, which reveals a diagonal band of low bias regions at intermediate values of  $\delta_8$  and  $\alpha_5$ .

However, despite the high level of complexities in the observed cosmic web dependences of  $w_p$ , they can all be very closely reproduced by our simple iHOD galaxy mock with no inbuilt cosmic web effects on galaxy clustering. We constrain the rms of slope of any additional dependence of relative bias on  $\alpha_5$  to be  $\sigma_{m_{\alpha_5}} = 0.30$ . Therefore any model producing  $m_{\alpha_5} > 0.9$  is ruled out for our sample at the  $3\sigma$  significance level. We obtain  $m_{\alpha_5} = 0.69 \pm 0.30$  for our iHOD mock galaxy catalogue. This could be taken as providing some weak evidence of cosmic web effects on the spatial clustering of galaxies, implying that the stellar-to-halo mass relation and the HOD of satellite galaxies might depend on the local tidal field. But this could as well be due the fact that we work in apparent redshift space and the peculiar velocity in the mocks are not modelled accurately. Some preliminary test shows that strong difference in peculiar velocity could produce such a deviation.

As a statistical measure of quenching, the mean  $g-r$  colour of SDSS galaxies is a strong function of  $\delta_8$ , with some subtle but non-trivial dependence on  $\alpha_5$  at fixed  $\delta_8$ . We also examined the relative clustering of red vs. blue galaxies across different  $\delta_8$  and  $\alpha_5$  regions, which probes the spatial segregation of the two colours in each region. Remarkably, the observed dependences of galaxy mean colour and colour segregation are in excellent agreement with the predictions from the iHOD fiducial halo quenching model, including the subtle mean colour dependence on  $\alpha_5$  and the characteristic scale at which the relative clustering starts deviating from unity. This agreement is encouraging news for the theoretical interpretation of galaxy quenching in the halo model, as the tidal tensor field can be largely ignored when modelling the colour transformation of galaxies.

Our analysis could be affected by a few systematic uncertainties in the measurement. In particular, our compact characterization of the cosmic web could be overly simplistic, and therefore may not capture the full properties of the tidal tensor field. For instance, the tidal field may operate on galaxy formation over a smaller distance scale than  $5 h^{-1} \text{Mpc}$ , the one we used for defining  $\alpha_5$ . However, we expect a strong correlation between the tidal anisotropies defined at various different scales below the correlation length of galaxy clusters (Croft et al. 1997). Therefore, the use of  $\alpha_5$  may not be optimal, but the effect of tidal anisotropy should nonetheless show up in our analysis if a strong cosmic web effect on clustering and/or quenching indeed exists. Another potential source of systematic error is the modelling of peculiar velocities in the mock. We have implemented the best-fitting velocity bias model of Guo et al. (2015a), which assumes that the relative velocities of central and satellite galaxies follow Gaussian distributions within each halo. However, the velocity distribution of galaxies has some level of anisotropy that is likely to be correlated with the tidal anisotropy outside the halo, especially in massive clusters (Zu & Weinberg 2013). We expect that the problem can be at least partially resolved in the future by directly using the velocities of subhaloes, which would require a simulation of higher resolution than Bolshoi.

Theoretically speaking, the success of the simple iHOD halo

quenching model further strengthens the argument that the halo mass plays the primary role in shaping the galaxy content inside individual dark matter haloes. Similarly, the lack of strong cosmic web effects on the colour transformation of galaxies implies that the galaxy quenching is a relatively local process that is contained within the boundary of haloes (Baxter et al. 2017), and that the tidal modulation of the large-scale cold gas accretion is unlikely to be the controlling factor triggering galaxy quenching. An exciting prospect is to apply a similar analysis to the cosmic web at higher redshifts (e.g., DESI; DESI Collaboration et al. 2016), as hydrodynamic simulations predict that the temperature distribution of the gas accretion becomes more bimodal with increasing redshift (Kereš et al. 2005).

While this work was being completed, we became aware of a related analysis by Paranjape et al. (2018). These authors have analysed the tidal environment of SDSS galaxies using a different set of selection criteria, analysis techniques, and definition of tidal anisotropy, and focused exclusively on the dependence of galaxy clustering on tidal anisotropy. Encouragingly, the results of our two independent analyses on the cosmic web dependences of galaxy clustering, wherever they can be compared, are qualitatively consistent.

## ACKNOWLEDGMENTS

We thank David H. Weinberg for helpful discussions. We would like to thank Uros Seljak, Sukhdeep Singh and Hung-Jin Huang for comments and discussion on the bias measurement and the importance of cross-correlations. We would also like to thank Simon White and Katarina Kraljic for useful comments on an earlier version of the draft. SA and JAP are supported by the European Research Council through the COSFORM Research Grant (#670193). YZ is supported by a CCAPP fellowship and the Thousand Talents Program of China. We thank the Bolshoi team for making their simulations publicly available. This research has made use of the NASA/IPAC Extragalactic Database (NED) which is operated by the Jet Propulsion Laboratory, California Institute of Technology, under contract with the National Aeronautics and Space Administration. This research has made use of NASA's Astrophysics Data System.

## REFERENCES

- Abazajian K. N., et al., 2009, *ApJS*, **182**, 543
- Abbas U., Sheth R. K., 2007, *MNRAS*, **378**, 641
- Alonso D., Eardley E., Peacock J. A., 2015, *MNRAS*, **447**, 2683
- Alpaslan M., et al., 2016, *MNRAS*, **457**, 2287
- Aragon-Calvo M. A., Neyrinck M. C., Silk J., 2016, preprint, ([arXiv:1607.07881](https://arxiv.org/abs/1607.07881))
- Baxter E., et al., 2017, *ApJ*, **841**, 18
- Behroozi P. S., Wechsler R. H., Wu H.-Y., 2013, *ApJ*, **762**, 109
- Benson A. J., Cole S., Frenk C. S., Baugh C. M., Lacey C. G., 2000, *MNRAS*, **311**, 793
- Berlind A. A., Weinberg D. H., 2002, *ApJ*, **575**, 587
- Blanton M. R., et al., 2005, *AJ*, **129**, 2562
- Bond J. R., Kofman L., Pogosyan D., 1996, *Nature*, **380**, 603
- Borzyszkowski M., Porciani C., Romano-Díaz E., Garaldi E., 2017, *MNRAS*, **469**, 594
- Bray A. D., et al., 2016, *MNRAS*, **455**, 185
- Bruzual G., Charlot S., 2003, *MNRAS*, **344**, 1000
- Calderon V. F., Berlind A. A., Sinha M., 2017, preprint, ([arXiv:1712.02797](https://arxiv.org/abs/1712.02797))



- Castorina E., Paranjape A., Hahn O., Sheth R. K., 2016, preprint, ([arXiv:1611.03619](https://arxiv.org/abs/1611.03619))
- Catelan P., Theuns T., 1996, *MNRAS*, **282**, 436
- Cattaneo A., Dekel A., Devriendt J., Guiderdoni B., Blaizot J., 2006, *MNRAS*, **370**, 1651
- Chabrier G., 2003, *PASP*, **115**, 763
- Chen Y.-C., et al., 2017, *MNRAS*, **466**, 1880
- Cooray A., Sheth R., 2002, *Phys. Rep.*, **372**, 1
- Correa C. A., Schaye J., Wyithe J. S. B., Duffy A. R., Theuns T., Crain R. A., Bower R. G., 2018, *MNRAS*, **473**, 538
- Croft R. A. C., Dalton G. B., Efstathiou G., Sutherland W. J., Maddox S. J., 1997, *MNRAS*, **291**, 305
- Crone Odekon M., Hallenbeck G., Haynes M. P., Koopmann R. A., Phi A., Wolfe P.-F., 2017, preprint, ([arXiv:1712.05045](https://arxiv.org/abs/1712.05045))
- Croton D. J., Gao L., White S. D. M., 2007, *MNRAS*, **374**, 1303
- DESI Collaboration et al., 2016, preprint, ([arXiv:1611.00036](https://arxiv.org/abs/1611.00036))
- Davis M., Geller M. J., 1976, *ApJ*, **208**, 13
- Dekel A., Birnboim Y., 2006, *MNRAS*, **368**, 2
- Dressler A., 1980, *ApJ*, **236**, 351
- Eardley E., et al., 2015, *MNRAS*, **448**, 3665
- Forero-Romero J. E., Hoffman Y., Gottlöber S., Klypin A., Yepes G., 2009, *MNRAS*, **396**, 1815
- Guo H., et al., 2015a, *MNRAS*, **453**, 4368
- Guo Q., Tempel E., Libeskind N. I., 2015b, *ApJ*, **800**, 112
- Guo H., Li C., Zheng Z., Mo H. J., Jing Y. P., Zu Y., Lim S. H., Xu H., 2017, *ApJ*, **846**, 61
- Hahn O., Porciani C., Carollo C. M., Dekel A., 2007, *MNRAS*, **375**, 489
- Hahn O., Porciani C., Dekel A., Carollo C. M., 2009, *MNRAS*, **398**, 1742
- Heavens A., Peacock J., 1988, *MNRAS*, **232**, 339
- Henriques B. M. B., White S. D. M., Thomas P. A., Angulo R., Guo Q., Lemson G., Springel V., Overzier R., 2015, *MNRAS*, **451**, 2663
- Jing Y. P., Mo H. J., Börner G., 1998, *ApJ*, **494**, 1
- Kaiser N., 1984, *ApJ*, **284**, L9
- Kauffmann G., et al., 2003, *MNRAS*, **341**, 33
- Kauffmann G., Li C., Zhang W., Weinmann S., 2013, *MNRAS*, **430**, 1447
- Kereš D., Katz N., Weinberg D. H., Davé R., 2005, *MNRAS*, **363**, 2
- Kleiner D., Pimbblet K. A., Jones D. H., Koribalski B. S., Serra P., 2017, *MNRAS*, **466**, 4692
- Klypin A. A., Trujillo-Gomez S., Primack J., 2011, *ApJ*, **740**, 102
- Kraljic K., et al., 2017, preprint, ([arXiv:1710.02676](https://arxiv.org/abs/1710.02676))
- Kravtsov A. V., Berlind A. A., Wechsler R. H., Klypin A. A., Gottlöber S., Allgood B., Primack J. R., 2004, *ApJ*, **609**, 35
- Kuutma T., Tamm A., Tempel E., 2017, *A&A*, **600**, L6
- Landy S. D., Szalay A. S., 1993, *ApJ*, **412**, 64
- Leauthaud A., Tinker J., Behroozi P. S., Busha M. T., Wechsler R. H., 2011, *ApJ*, **738**, 45
- Libeskind N. I., et al., 2018, *MNRAS*, **473**, 1195
- Lin Y.-T., Mandelbaum R., Huang Y.-H., Huang H.-J., Dalal N., Diemer B., Jian H.-Y., Kravtsov A., 2016, *ApJ*, **819**, 119
- Ma C.-P., Fry J. N., 2000, *ApJ*, **543**, 503
- Malavasi N., et al., 2017, *MNRAS*, **465**, 3817
- Mandelbaum R., Seljak U., Kauffmann G., Hirata C. M., Brinkmann J., 2006, *MNRAS*, **368**, 715
- Mandelbaum R., Wang W., Zu Y., White S., Henriques B., More S., 2016, *MNRAS*, **457**, 3200
- McEwen J. E., Weinberg D. H., 2016, preprint, ([arXiv:1601.02693](https://arxiv.org/abs/1601.02693))
- Metuki O., Libeskind N. I., Hoffman Y., Crain R. A., Theuns T., 2015, *MNRAS*, **446**, 1458
- Musso M., Cadiou C., Pichon C., Codis S., Kraljic K., Dubois Y., 2018, *MNRAS*, **473**, 1195
- Oemler Jr. A., 1974, *ApJ*, **194**, 1
- Paranjape A., Hahn O., Sheth R. K., 2017, preprint, ([arXiv:1706.09906](https://arxiv.org/abs/1706.09906))
- Paranjape A., Hahn O., Sheth R. K., 2018, preprint, ([arXiv:1801.04568](https://arxiv.org/abs/1801.04568))
- Peacock J. A., Smith R. E., 2000, *MNRAS*, **318**, 1144
- Peebles P. J. E., 1980, The large-scale structure of the universe
- Poudel A., Heinämäki P., Tempel E., Einasto M., Lietzen H., Nurmi P., 2017, *A&A*, **597**, A86
- Sales L. V., et al., 2015, *MNRAS*, **447**, L6
- Salim S., et al., 2007, *ApJS*, **173**, 267
- Scoccimarro R., Sheth R. K., Hui L., Jain B., 2001, *ApJ*, **546**, 20
- Seljak U., 2000, *MNRAS*, **318**, 203
- Sheth R. K., 1998, *MNRAS*, **300**, 1057
- Sheth R. K., Tormen G., 1999, *MNRAS*, **308**, 119
- Sin L. P. T., Lilly S. J., Henriques B. M. B., 2017, preprint, ([arXiv:1702.08460](https://arxiv.org/abs/1702.08460))
- Sunyaev R. A., Zel'dovich Y. B., 1972, *A&A*, **20**, 189
- Sutter P. M., et al., 2015, *Astronomy and Computing*, **9**, 1
- Tinker J. L., Conroy C., Norberg P., Patiri S. G., Weinberg D. H., Warren M. S., 2008, *ApJ*, **686**, 53
- Tinker J. L., Hahn C., Mao Y.-Y., Wetzel A. R., Conroy C., 2017, preprint, ([arXiv:1702.01121](https://arxiv.org/abs/1702.01121))
- Tojeiro R., et al., 2017, *MNRAS*, **470**, 3720
- Wang L., Weinmann S. M., De Lucia G., Yang X., 2013, *MNRAS*, **433**, 515
- Wang H., et al., 2016, *ApJ*, **831**, 164
- White S. D. M., Frenk C. S., Davis M., Efstathiou G., 1987, *ApJ*, **313**, 505
- Wibking B. D., et al., 2017, preprint, ([arXiv:1709.07099](https://arxiv.org/abs/1709.07099))
- Xia Q., Kang X., Wang P., Luo Y., Yang X., Jing Y., Wang H., Mo H., 2017, *ApJ*, **848**, 22
- Yan H., Fan Z., White S. D. M., 2013, *MNRAS*, **430**, 3432
- Yang X., Mo H. J., van den Bosch F. C., 2003, *MNRAS*, **339**, 1057
- Yang X., et al., 2017a, preprint, ([arXiv:1712.00883](https://arxiv.org/abs/1712.00883))
- Yang X., et al., 2017b, *ApJ*, **848**, 60
- York D. G., et al., 2000, *AJ*, **120**, 1579
- Zehavi I., Contreras S., Padilla N., Smith N. J., Baugh C. M., Norberg P., 2017, preprint, ([arXiv:1706.07871](https://arxiv.org/abs/1706.07871))
- Zel'dovich Y. B., 1970, *A&A*, **5**, 84
- Zentner A. R., Hearin A., van den Bosch F. C., Lange J. U., Villarreal A., 2016, preprint, ([arXiv:1606.07817](https://arxiv.org/abs/1606.07817))
- Zheng Z., et al., 2005, *ApJ*, **633**, 791
- Zu Y., Mandelbaum R., 2015, *MNRAS*, **454**, 1161
- Zu Y., Mandelbaum R., 2016, *MNRAS*, **457**, 4360
- Zu Y., Mandelbaum R., 2017, preprint, ([arXiv:1703.09219](https://arxiv.org/abs/1703.09219))
- Zu Y., Weinberg D. H., 2013, *MNRAS*, **431**, 3319
- Zu Y., Zheng Z., Zhu G., Jing Y. P., 2008, *ApJ*, **686**, 41
- Zu Y., Mandelbaum R., Simet M., Rozo E., Rykoff E. S., 2017, *MNRAS*, **470**, 551
- van de Weygaert R., 2012, in Proceedings of the Twenty-eighth Annual Symposium on Computational Geometry. SoCG '12. ACM, New York, NY, USA, pp 311–312, doi:10.1145/2261250.2261296, <http://doi.acm.org/10.1145/2261250.2261296>